



THE UNIVERSITY OF QUEENSLAND
AUSTRALIA

Early stage yield prediction in lettuce using analysis of images from unmanned aerial vehicles (UAVs)

Binyin Patrick Di



0000-0002-0289-8016

*A thesis submitted for the degree of Bachelor of Agricultural Science (Honours)
at The University of Queensland in Year 2020*

School of Agriculture and Food Sciences

AGRC4614 Research Project

November 2020



Aerial view of the fields located at Koala Farms, Lake Clarendon, Queensland, Australia.

ABSTRACT

Lettuce (Lactuca sativa L.) is an essential horticultural crop in Australia. Biomass and plant dimensions are fundamental traits for the evaluation of crop production and yield for lettuce. The aim of this study was to 1) estimate measurements of plant dimensions (area and volume) by biomass at any particular time of the season, 2) predict final biomass from plant dimensions at earlier stages of the crop, and 3) interpret physiological differences in growth rate during seasons of production, such as fraction of light interception (fINT) and light use efficiency (LUE).

The UAV was flown regularly over the paddocks throughout two seasons (transplanted on 9 April and 19 May) of production and destructive samples were taken to measure the fresh biomass, and samples dried to determine dry biomass. In the final harvest, each lettuce was weighed for total biomass, market-standard biomass and core biomass after two trimming processes. Across multiple harvests, the masking of plants from images using a thresholding technique was visually accurate, up to the point where plants were beginning to overlap each other.

For successive temporal observations through the season, we compared the plant area to biomass on the same day. The best results for these comparisons were at 26 days after transplanting (DAT) with adjusted $R^2 = 0.79$ in Season 1 and 16 DAT with adjusted $R^2 = 0.67$ in Season 2 for plant area against biomass. We also compared the plant biovolume to biomass, the results in Season 1 does not show significant adjusted R^2 values, but at 38 DAT in Season 2 with adjusted $R^2 = 0.62$. To meet Aim 2, the best prediction of final biomass (adjusted $R^2 = 0.42$ for Season 1 and adjusted $R^2 = 0.54$ for Season 2) were found to be obtained from UAV estimates of plant area at about 400 °Cd (~ 22-24 DAT). For biovolume against biomass in prediction models, the best fits were at 22 DAT with adjusted $R^2 = 0.35$ in Season 1 and 38 DAT with adjusted $R^2 = 0.59$ in Season 2. Across the multiple harvests and flights, it was evident that canopy development and fINT was slower to increase in the cooler season when compared on calendar time. By estimating light interception and using observed biomass, we were able to show that the crops had a similar LUE in both seasons. The marketable harvest index (MHI) presented the marketable part to total biomass showing there was a large variability amongst lettuce individuals due to lettuce big-vein virus disease pressure.

UAV predictions of fresh biomass of lettuce on the day of the flight or for a future flight were only moderate in precision. However, UAV estimates of fINT were sufficient to improve predictions of biomass at a future date by summing the product of incident radiation, estimated fINT and a constant LUE. Hence, there is the potential to project fINT profiles for a season and estimate final fresh biomass. However, to estimate marketable biomass, we need to make more to understand how core development occurs and how MHI changes with different stages of growth.

DECLARATION BY AUTHOR

This thesis describes the original work of the author and contains no material previously published or written by another person except where due reference has been made in the text. It has not been submitted previously for the award of a degree at any university.

ACKNOWLEDGEMENTS

Special thanks to the following people supporting me throughout the project:

- Prof Scott Chapman (Supervisor, School of Agriculture and Food Sciences)
- Dr Vincent Mellor (Biometrician consultant, School of Agriculture and Food Sciences)
- Mr Daniel Smith (Colleague, School of Agriculture and Food Sciences)
- Mr Alex Chamanmáh (Colleague, School of Agriculture and Food Sciences)
- Mr Chrisbin James (Colleague, School of Information Technology and Electrical Engineering)
- Dr Bangyou Zheng (Collaborator, CSIRO)
- Mr Nat Parker (Collaborator, AirBorn Insight Pty Ltd)
- Mr Anthony Staatz (CEO Koala Farms)
- Mr Luke Spittle (Collaborator, Koala Farms)
- Ms Connar McLaren (Technical Staff)
- Ms Bec Archer (Technical Staff)
- Ms Cheryl Brugman (Student Services)

TABLE OF CONTENTS

Abstract	I
Declaration by author	II
Acknowledgements	III
List of Tables	VII
List of Figures	VII
List of Plates	IX
1. Introduction	1
2. Literature Review	2
2-1. Background	2
2-2. Unmanned Aerial Vehicles and estimation of crop cover (plant area)	2
2-3. Crop models	3
2-4. Biomass composition	4
2-4-1. Water	4
2-4-2. Structural and non-structural biomass.....	5
2-5. Biomass formation	5
2-5-1. Leaf area development and growth form	5
2-5-2. Intercepted radiation.....	6
2-5-3. Light Use Efficiency (LUE).....	7
2-5-4. Light extinction coefficient	7
2-6. Lettuce responses to environment.....	8
2-6-1. Plant response to climate change	8
2-6-2. Plant response to the temperature.....	8
2-6-3. Lettuce response to the temperature	9
2-7. Transplant shock	9

2-8.	Harvest index and yield formation.....	10
2-9.	Potential diseases	11
3.	Materials and Methods	12
3-1.	Study site.....	12
3-2.	Cultivars, experimental design and layout scheme.....	13
3-3.	Destructive sampling	14
3-4.	Marketable Harvest Index, Water Content, Light Use Efficiency.....	15
3-5.	Thermal time	16
3-6.	RGB imagery analysis	17
3-7.	Ground Sample Distance	18
3-8.	Image processing	19
3-9.	Image feature extraction	20
3-10.	Biovolume estimation	21
3-11.	Lettuce biomass simulation.....	21
3-12.	Statistical analysis	22
4.	Results.....	23
4-1.	Environmental conditions	23
4-2.	Crop growth models over thermal time	26
4-2-1.	Plant biomass accumulation	27
4-2-2.	Fraction of intercepted radiation	28
4-2-3.	Plant volume expansion	28
4-2-4.	Plant dry matter accumulation.....	29
4-2-5.	Water content	29
4-3.	Correlations between plant area and plant biomass.....	30
4-3-1.	Real-Time models	30
4-3-2.	Prediction models.....	31
4-4.	Correlations between plant biovolume and plant biomass	34
4-4-1.	Real-Time models	34

4-4.2. Prediction models	35
4-5. Marketable Harvest Index (MHI)	37
4-6. Light interception and Light Use Efficiency (LUE)	39
4-7. Lettuce growth simulation	41
5. Discussion	46
5-1. Growing conditions.....	46
5-2. Biomass accumulation and growth rates.....	46
5-3. Lettuce growth simulation	47
5-4. Lettuce simulation and effects of seeding size and transplant shock.....	48
5-5. Crop modelling on lettuce.....	49
5-6. Remote sensing applications.....	50
5-7. Disease impact on lettuce biomass production	50
5-8. Marketable Harvest Index (MHI)	50
5-9. Future research directions	51
6. Conclusion	52
7. References	53
8. Appendix	62

LIST OF TABLES

Table 3-1 Experimental layout * lettuce samples harvested; red highlighted: lettuce samples dehydrated.	13
Table 3-2 Specifications of DJI Phantom 4 Advanced were used to calculated GSD, collected from (DJI n.d.).....	18
Table 3-3 Three steps in image feature extraction	20
Table 4-1 Fitted curves for crop growth by fresh biomass (g/plant), the fraction of intercepted radiation (fINT, -), biovolume (m ³ /m ²), dry matter (g/plant) and water content (per plant) against Cumulative Thermal Time (°Cd).....	26
Table 4-2 Summary of models to predict fresh biomass from the final harvest of 48 plants using the estimated plant area of those same plants for each flight date, The cumulative thermal time started from the date of transplanting. • Season 1 harvests; ▫ Season 2 harvests.....	31
Table 4-3 Classifications of lettuce based on biomass.....	38
Table 4-4 Summary of the relationships between Light Use Efficiency (LUE) and Average Temperature (AvgTemp) on lettuce in the early stages and the whole growth stages.....	41
Table 4-5 Fitted curves for crop growth by fraction of intercepted radiation (fINT, -), Cumulative Intercepted Solar Radiation (CumINTR) and water content (per plant) against Cumulative Thermal Time (°Cd).	41
Table 4-6 Recalculated Light Use Efficiency when $T_b = 7\text{ }^\circ\text{C}$	43

LIST OF FIGURES

Figure 2-1 An overview of ten typical lettuce phenology, adapted from Jenni and Bourgeois (2008).	6
Figure 2-2 Changes of Harvest Index of wheat, barley and rice varieties over a century, adapted from Evans (1993).....	10
Figure 3-1 Site location with paddock sizes for two growing seasons.	13
Figure 3-2 Flow diagram outlining the destructive sampling process.	15
Figure 3-3 Visual representation of calculating GSD, adopted from Propeller Aero (2018). .	19
Figure 3-4 An orthomosaic image of a flight with GCPs and image points was produced in Agisoft.....	19
Figure 3-5 Calculating volumes lettuce by drawing polygons (bounding boxes) around each individual.....	21
Figure 4-1 Seasonal weather conditions of Season 1 including daily minimum and maximum temperature, solar radiation along with precipitation over thermal time.	24
Figure 4-2 Seasonal weather conditions of Season 2 including daily minimum and maximum	

VIII

temperature, solar radiation along with precipitation over thermal time.	25
Figure 4-3 Cumulative thermal time and cumulative solar radiation for • Season 1 and ◻ Season 2.	26
Figure 4-4 Plant Fresh Biomass was plotted against Cumulative Thermal Time in contrasting seasons fitted with logistic regression. The relative cumulative thermal time started from the first harvest.	27
Figure 4-5 Fraction of Intercepted Radiation was plotted against Cumulative Thermal Time in contrasting seasons fitted with exponential curves started from the dates of transplanting. (maximum fraction of intercepted radiation = 1)	28
Figure 4-6 Plant Volume was plotted against Cumulative Thermal Time in contrasting seasons fitted with exponential curves started from the first harvest.	28
Figure 4-7 Plant Dry Weight was plotted against Cumulative Thermal Time in contrasting seasons fitted with logistic regression started from the first harvest.	29
Figure 4-8 Water Content was plotted against Cumulative Thermal Time in contrasting seasons fitted with logistic regression started from the first harvest.	29
Figure 4-9 The correlations between fresh biomass of harvest plots from each harvest and plant area of harvest plots from each flight in Season 1 fitted with linear regression.	30
Figure 4-10 The correlations between fresh biomass of harvest plots from each harvest and plant area of harvest plots from each flight in Season 2 fitted with linear regression.	31
Figure 4-11 Adjusted R-squared values from the above models were plotted against Cumulative Thermal Time. • Season 1; ◻ Season 2	32
Figure 4-12 Fresh biomass from the final harvest was plotted against plant area of final harvest plots over each flight in Season 1 fitted with linear regression.	33
Figure 4-13 Fresh biomass from the final harvest was plotted against the plant area of final harvest plots over each flight in Season 2 fitted with linear regression.	33
Figure 4-14 The correlations between fresh biomass and plant biovolume of each harvest plots in Season 1 fitted with linear regression.	34
Figure 4-15 The correlations between fresh biomass and plant biovolume of each harvest plots in Season 2 fitted with linear regression.	35
Figure 4-16 The correlations between fresh biomass and plant biovolume of final harvest plots in Season 1 fitted with linear regression.	36
Figure 4-17 The correlations between fresh biomass and plant biovolume of final harvest plots in Season 2 fitted with linear regression.	36
Figure 4-18 Plants from final harvest in each season were ranked based on Market Standard Trimmed Biomass (L), Labels: Plant ID. Marketable Harvest Index (MHI) in contrasting	

seasons (R).	37
Figure 4-19 Plant Core Biomass was plotted against Core/Total Biomass Ratio for Season 2 fitted with linear regression.	38
Figure 4-20 Intercepted radiation was plotted against Cumulative Thermal Time fitted with the expo-linear model from the first harvest.	39
Figure 4-21 The relationships between dry matter difference and intercepted solar radiation for two seasons at early stages and whole growth stages fitted with linear regression.	40
Figure 4-22 Fraction of Intercepted Radiation and Water Content (Quasi- R^2 : 0.79) were plotted against Cumulative Thermal Time in contrasting seasons fitted with exponential curves started from the dates of transplanting when $T_b = 7^\circ\text{C}$. (maximum fraction of intercepted radiation = 1).....	42
Figure 4-23 Intercepted radiation was plotted against Cumulative Thermal Time fitted with the expo-linear model when $T_b = 7^\circ\text{C}$	42
Figure 4-24 The relationships between dry matter difference and intercepted solar radiation for two seasons at early stages and whole growth stages fitted with linear regression, when $T_b = 7^\circ\text{C}$	43
Figure 4-25 Fresh biomass was simulated from 2001 to 2020, when $T_b = 7^\circ\text{C}$ for Season 1 over different (40, 50, 60, 70 DAT) periods of growth after transplanting.....	44
Figure 4-26 Fresh biomass was simulated from 2001 to 2020, when $T_b = 7^\circ\text{C}$ for Season 2 over different (40, 50, 60, 70 DAT) periods of growth after transplanting.....	45
Figure 4-27 Fresh Biomass was simulated against average temperature over a 20-year period. Labels: 20yy format of years.....	45
Figure 5-1 The correlations between fresh biomass and cumulative intercepted solar radiation fitted with linear regression.	47
Figure 5-2 Aerial view of lettuce plants after three weeks after transplanting. Circled: blue-smaller than average size, purple- average size, red- larger than average size.	48
Figure 5-3 Trends of fINT against Cumulative Thermal Time of three sizes of lettuce (fINT: 50% smaller, Average size, 50% larger)	49

LIST OF PLATES

Plate 3-1 Setting up the two devices in the paddock (top: time-lapse camera; bottom: Arable Mark 2 sensor).....	12
Plate 3-2 Phantom 4 Advanced with an RGB camera sitting on a GCP mat.	17
Plate 3-3 Flights path in 10m, 20m and 40m respectively.	18

1. INTRODUCTION

Lettuce, *Lactuca sativa* L., is a main ingredient of salad all over the world. Lettuce is ranked as Australia's 5th largest vegetable by production volume (136,937 metric tonnes) in 2018/2019, amounting to AU\$172.8 million in overall production (Hort Innovation 2019). Iceberg lettuce, also known as Crisphead or Saladin, is the most popular cultivar commercially grown in Australia followed by Butterhead, Cos (Romaine) and Loose leaf (Deuter *et al.* 2012; Carey *et al.* 2017), and is well-suited to growing conditions in Lockyer Valley and East Darling Downs (Queensland), Gippsland (Victoria) and Sydney Basin (New South Wales) (Hort Innovation 2019).

Although augmented by rigorous management including careful irrigation and nutrition programmes, field lettuce production is impacted by temperature, radiation and pest and disease challenges. Additionally, one of the major costs for growers is labour required at harvest. Growers could benefit from knowing the best time to harvest the crop, in order to maximise the number of marketable heads taken at harvest. Repeated harvests incur additional expenses, and poor harvest timing can result in large losses when plants are abandoned in the field.

Unmanned Aerial Vehicles (UAVs) offer the potential to characterise crop size over time, and to assist growers in managing these harvest time issues. The work presented here aims to answer the following questions:

1. Can biomass be estimated directly from measurements of plant dimensions (area and volume) at any particular time of the season?
2. Is final biomass correlated with plant dimensions at earlier stages of the crop?
3. What physiological differences exist in growth rate during different seasons of production, *eg* related to light interception and light use efficiency?

2. LITERATURE REVIEW

2-1. Background

Crop biomass, a crucial measure of plant growth, is defined as the dry weight of plant matter per unit area and is impacted by environmental factors (*eg* water stress, nutrient supply, soil quality) and agricultural management practices within a growth cycle (Bendig *et al.* 2014; Bendig *et al.* 2015; Ballesteros *et al.* 2018). Based on crop biomass in a large scale of spatiality and temporality, an accurate and efficient crop yield prediction is one of the major constraints for management and market decision-making, including harvest timing (Ballesteros *et al.* 2018).

2-2. Unmanned Aerial Vehicles and estimation of crop cover (plant area)

Unmanned Aerial Vehicles (UAVs), are a popular platform for inspection, surveillance, mapping and 3D modelling missions (Nex & Remondino 2014). This novel approach is prone to deliver timely, systematically high-quality forecast and information in contrast to the conventional ground-based crop survey (Noureldin *et al.* 2013; Zhou *et al.* 2017). Acquiring data across growing seasons, imagery from a variety of cameras can be used to inspect the crop growth at multiple times in a large scale for remote sensing (RS), to inform near real-time decision making. Additionally, this method not only is capable to provide high-resolution spatial data, but also is non-destructive and less intrusive in comparison to other current technologies.

Viewed from a nadir position, crop cover, that is the fraction of the area covered by the crop to the total soil surface area, is linked to affect the crop radiation capture [canopy photosynthetic rate (distribution and interception of light) and actual evapotranspiration], water-use efficiency and yield (Duan *et al.* 2017). The previous research has shown at early stages while the vegetative cover is little, evaporation rate is dominated by the soil and as crop cover is expanding, the evaporation rate is more dependent on the leaf area (Ritchie 1972). Crop cover is also a parameter in estimation of crop coefficients, that predict actual evapotranspiration relative to a standardised grass surface and further estimate water uptake and use throughout the growing season (Duan *et al.* 2017).

The most common method to estimate the crop cover is using a simple three-channel RGB (Red Green Blue) camera that is mounted on the drone. The estimation is simply achieved by separating and classifying image pixels into two categories: the plant objects and non-plant objects (residuals) through semantic image segmentation, also called as pixel-level classification. It is the process of partitioning a digital image into multiple segments (sets of pixels also known as super pixels) (Raju & Neelima 2012). It simplifies the image analysis by clustering the parts of images, that belong to the same object class, into an appropriate plane, where the pixels can be distinctly separated by a pre-calculated threshold value (Guo *et al.* 2013; Liu *et al.* 2019). However, it may require different user-defined colour thresholds for every image because the values are highly dependent upon the light conditions (*eg* specularly reflected parts and shadowed parts on chromatic features) (Guo *et al.* 2013). Thresholding is the most common and simple method of segmenting images to estimate foreground against the background in a binary image. The homogeneous and contiguous pixels (called objects) could be grouped by the Object Based Image Analysis (OBIA), which reduces intra-class spectral variability and the background noise, such as shadows, gaps etc (Torres-Sánchez *et al.* 2015). Then, the imported values in the colour channel could be treated by Classification and Regression Trees (CART), a decision tree developed by Breiman *et al.* (1984). Thus, the thresholding and segmentation of per-pixel of each vegetation could be achieved by following steps outlined in Guo *et al.* (2013): “(1) Acquisition of a training data set from training images to train the model.(2) Training of the model to create a decision tree using the training data set.(3) Vegetation segmentation of test images using the decision tree. (4) Noise reductions on the segmented test images.”

2-3. Crop models

Crop models, defined as a “schematic representation of the system” as stated by De Wit (1969), play an important role in two broad areas of agriculture. First, is the “enhanced heuristic role” of models in crop management decisions, scientific investigation, education and issue-solving on land policy. Second is an “increasing role” of models concerning crop genetic regulation and anticipated responses to genetic alterations (Hammer *et al.* 2002).

Crop yield prediction is created by statistical analysis from either experimental datasets (*eg* Thornthwaite's formula of potential evapotranspiration, ETP) or physical laws (*eg* Penman's formula of ETP) (Gary *et al.* 1998). The statistical approach is based on three types of approaches found in the literature: time series methods, panel methods and cross-section methods, which rely upon purely time series that are more advantageous yet limited by data, both time and space, and solely space variations respectively (Lobell & Burke 2010).

The first lettuce growth simulation with a biophysical model was conducted by Soribe and Curry (1973) using time series methods in an air-supported plastic greenhouse. Later in 1994, a dynamic 4-dimensional growth model was firstly developed by van Henten (1994) under greenhouse climate. It explained several climatic factors, *ie* the active photosynthetic radiation, the carbon dioxide concentration and the air temperature, which can affect both structural and non-structural dry weights in the greenhouse condition (van Henten 1994). The first order sensitivity test from this model expressed that a few parameters determine the lettuce growth. These parameters include the yield factor, which is responsible for respiratory and synthesis losses of non-structural material compensated by the rapid growth of structural material, the extinction coefficient of canopy, the leaf area ratio, the light use efficiency (LUE) of leaf photosynthesis and maximum growth rate coefficient, and some which only affect during a limited time (van Henten 1994). The most recent model of lettuce prediction in Japan utilised Gompertz function with three coefficients fitted to the lettuce growth under greenhouse condition. It was found that the model has a typical growth curve, whose two coefficients are related to experimental conditions and the other one is associated with fresh weight at harvest. Thus, fresh weight at harvest can be predicted from this one-parameter function (Shimizu *et al.* 2008).

$$\frac{1}{w} \frac{dw}{dw} = C_1 \exp(-C_2 t)$$

Equation 2-1

2-4. Biomass composition

2-4-1. Water

Water composes at least 85% fresh biomass for major green leafy vegetables (Gupta *et al.* 2013).

Plant growth relies on water for the following reasons: 1) it is a major constituent of physiologically active tissue; 2) it is a reagent in photosynthesis and hydrolytic processes; 3) it is the solvent for solute movement; and 4) it is essential and necessary for the maintenance of the turgidity, cell enlargement and growth (Kramer 1963). Thus, a plant must survive in the optimal range of plant water content (AW), defined as the difference between field capacity (FC) and wilting point (WP): $AW = FC - WP$ (Kirkham 2005). The current understanding of crop water use (also known as evapotranspiration, ET) for biomass production is based on the equation firstly proposed by de Wit (1958):

$$B = \frac{mT}{E_0}$$

Equation 2-2

Where, B is total crop biomass, m = crop constant, T = crop transpiration and E_0 = free water (potential) evaporation (Blum 2011).

2-4-2. Structural and non-structural biomass

Structural biomass, also known as lignocellulosic biomass, contains biopolymer matrix complex such as polysaccharides (*ie* cellulose, hemicellulose) and lignin. These are used to build three layers of cell walls for biomass recalcitrance, defined as “the resistance of plants to release their sugars for fermentation or upgrading” Gilna *et al.* (2017), by which the plant biomass is resistant to enzymatic and microbial deconstruction (Noureldin *et al.* 2013). In contrast, the non-structural biomass is composed of vegetative organic biomass and minerals. At the developmental stage of the different plant compartments during different times of a year, there are different outcomes of the distribution and assimilation between the structural and non-structural biomass (Gansert & Sprick 1998).

2-5. Biomass formation

2-5-1. Leaf area development and growth form

Lettuce growth stages can be classified into four main developmental growth stages: 1) germination, 2) leaf development, 3) head development, 4) inflorescence emergence (Jenni and Bourgeois (2008). (See Figure 2-1) Similarly, Raid (2004) categorised into three major stages

prior to harvest: 1) seedling development (20-36 days), 2) a rosette period (14-28 days), and 3) heading (26-56 days). At beginning of observation periods, leaves are produced in a rosette form from a central axis with the projected plant area increasing to create a ‘frame’ which is related to the proximity of other plants, *ie* to the planting density. In the latter period, the plant rapidly increases in weight (fills in the ‘frame’).

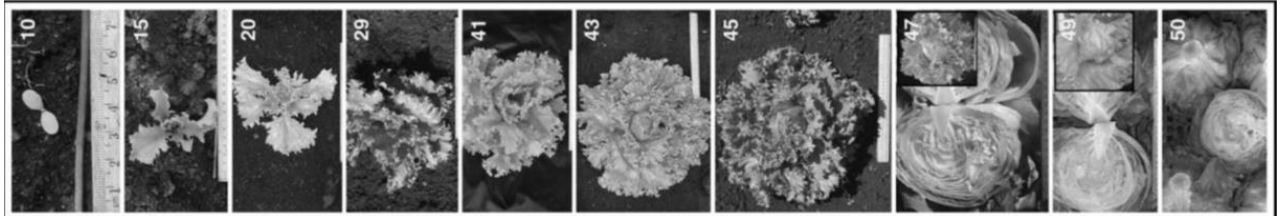


Figure 2-1 An overview of ten typical lettuce phenology, adapted from Jenni and Bourgeois (2008).

2-5-2. Intercepted radiation

Thermodynamically, the biomass production of a crop is based on the conversion fraction from energy input (solar radiation) to energy output (carbohydrate) stored through photosynthesis and from which the efficiency is defined (Monteith 1977). Over time (t , d), the accumulated dry matter (W g·m⁻²) in crops from assimilated carbon is directly proportional to daily incoming global intercepted radiation (Q , J·m⁻²·d⁻¹) with an integral equation (Monteith 1977; Wheeler *et al.* 1993a; Bouman 1995). In this equation, accumulated dry matter is linear to accumulated total intercepted radiation (i : the fraction of intercepted radiation, -); moreover, during the vegetative growth, the radiation conversion coefficient (ϵ , light use efficiency factor, g MJ⁻¹), which is the slope of this relationship, is symmetrically varied ($P < 0.001$) each harvest interval (Wheeler *et al.* 1993a).

$$W = \int \epsilon i Q dt$$

Equation 2-3

2-5-3. Light Use Efficiency (LUE)

From the seasonal and annual perspective, the absorbed photosynthetically active radiation (APAR) is proportional to NPP produced by the terrestrial ecosystem (Monteith 1972; Monteith 1977). Photosynthetically active radiation (PAR) utilisation efficiency, commonly known as light use efficiency (LUE, ϵ), is defined as the ratio of NPP to APAR (Haxeltine & Prentice 1996; Medlyn 1998). According to previous literature and experiments, the values of ϵ of many different species have been estimated, resulting in a wide range from 0.22 to 3.59 g MJ⁻¹ (Medlyn 1998).

$$NPP = \epsilon \text{ APAR}$$

Equation 2-4

The research from Fu *et al.* (2012) on lettuce under different light intensities (photosynthetic photon flux density, PPFD), showed the highest LUE (200 $\mu\text{mol m}^{-2}\text{s}^{-1}$) does not always correspond to the highest plant yield (600 $\mu\text{mol m}^{-2}\text{s}^{-1}$); hence, the authors suggested that 400-600* $\mu\text{mol m}^{-2}\text{s}^{-1}$ is preferred range for maximising economic benefits.

2-5-4. Light extinction coefficient

The definition of light extinction coefficient (K) is the “interception efficiency of light penetrating through the canopy as light intensity gradually decreases due to repeated attenuation by foliage elements” (Bisbis *et al.* 2018). In theory, K is determined by leaf inclined angle (α) and solar zenith angle (θ); and K can be calculated based on Beer-Lambert Law (Campbell 1986; Zhang *et al.* 2014; Bisbis *et al.* 2018):

$$K = -\frac{\ln\left(\frac{I_i}{I_o}\right) \cos\theta}{\text{LAI}\Omega};$$

or $S_b(L) = S_b(0) \exp(-KL)$;

or $k(\theta_s, \varphi_s) = G(\theta_s, \varphi_s) / \cos(\theta_s)$.

Equation 2-5

*400 $\mu\text{mol m}^{-2}\text{s}^{-1}$ is an optimal value set for supplementary light in winter greenhouse production of certain lettuce types in high latitude regions; 600 $\mu\text{mol m}^{-2}\text{s}^{-1}$ is an optimal value set for shading light in late spring and early autumn production of certain lettuce types in low latitude regions (Fu *et al.* 2012).

2-6. Lettuce responses to environment

2-6-1. Plant response to climate change

Crop production is highly influenced by the change of climatic processes [*ie* mean temperature change and shifts in precipitation patterns (hygrometry)]; also change of vegetation cover in different land use (Betts 2005). On a global scale, the model (Hybrid 6.5) projected that, by the end of this century, an increasing atmospheric CO₂ concentration and associated changes in climate will lead to increase 37.3% in net primary production (NPP). Besides, the mean increase of ranges from 43.9% to 52.9% NPP across various C₃ Generalized Plant Types (GPTs) in comparison to a 5.9% increase from C₄ plants (Friend 2010). For instance, the dry biomass and marketable yield of lettuce would be increasing 35-44%, if doubling the current level of CO₂ concentration (Streck 2005; Korres *et al.* 2016; Bisbis *et al.* 2018). The sensitivity test from the model also suggested the leaf phenology, which is referred to as the “arrangements of leaves in time (Kikuzawa 1995, p159)” as an aspect the light-harvesting strategy for plants, affects C₃ plant as well as needle-leaved cold deciduous tree production (Kikuzawa 1995; Friend 2010). Like other countries in the southern hemisphere, leaf phenology in Australia is driven by precipitation, which is more uncertain than temperature projection (Buitenwerf *et al.* 2015). It is common to see the plants in arid and semi-arid Australia, such as Murray Darling Basin, can skip an entire phenological cycle and vegetation fraction steadily declining in the peak year of drought; consequently, the land-surface energy balance (net radiation) was declining (Evans *et al.* 2017).

2-6-2. Plant response to the temperature

One of the most important processes for plant production is photosynthesis, a pathway for carbon fixation to harness energy from the sun by a light-dependent reaction, which was described by Calvin and Bassham (1962), later known as Calvin Cycle (Waller & Lewis 1979). The plant adaption in different temperature contributes to latitudinal and altitudinal distribution as well as various plant characteristics, such as plant height, leaf area, leaf geometry, photosynthetic capacity, and dark respiration (Öquist 1983; Anten 2004). In addition, Sage and Kubien (2007) summarised that photosynthesis can generally tolerate 0 —30 °C for plants which remain active in cold temperature or grow in high latitude and altitude areas with no harm, 7—40 °C safely for temperate or subtropical species from equitable habitats, and 15—

45 °C for tropical and summer plants without any apparent problems. In terms of optimal temperature requirement for CO₂ uptake, there is a distinction between C₃ and C₄ plants ranging from 10 to 25°C with a rapid decrease above 25°C for C₃ plants and 30 to 40°C decreasing harshly below 15 to 20°C for C₄ plants (Waller & Lewis 1979).

2-6-3. Lettuce response to the temperature

Like other C₃ plants, drought, particularly combined with high temperatures and high transpiration can not only reduce the yield but also cause a series of physiological disorders, such as bolting, tipburn, loose and puffy heads (Peet & Wolfe 2000; Sage & Zhu 2011). Air temperature in the ranges of 17-28°C during daytime and 3-12°C overnight are the most successful for lettuce production (Peet & Wolfe 2000). Likewise, as for the effects of mother-plant temperature and seeds on yield, medium production temperatures (25°C day, 15°C night) given medium-sized seeds provide the highest yield followed by high temperatures (30°C, 20°C) with smallest seeds and low temperatures (20 °C, 10 °C) with largest seeds (Drew & Brocklehurst 1990). Qin *et al.* (2002) found that a higher Root Zone Temperature (25-39°C-RZT) at early stages (*eg* before 11 DAT) and then transferring to 20°C-RZT performed better than a constant 20°C-RZT regarding the shoot productivity and root development. Otherwise, the growing period of 20°C-RZT is positively linear correlated to several production biomass parameters, including the total number of leaves, total leaf area, fresh and dry weights of shoot.

2-7. Transplant shock

Transplanting has several advantages that have been reviewed previously: it can generally optimise farm management for field cultivation (timing and scheduling), shorten the period for a more rapid growth cycle, enhance crop uniformity and phenological synchrony (flowering and fruiting), and boost yield and earliness (Qin & Leskovar 2020). However, it is inevitable, when a plant was moved from one to another, a plant could inevitably suffer transplant shock and associated stress due to improper transplanting techniques, the lack of pre-plant care or post-plant maintenance, such as mechanical damage of root tips and hairs, disturbance of root/shoot balance and transient root growth stunting (Gauthier *et al.* 2014; Qin & Leskovar 2020). Improving and sustaining a larger root system could lessen transplant shock and recover faster in lettuce (Weston & Zandstra 1986; Masson *et al.* 1991; Nicola & Cantliffe 1996). It

was reported that a lower leaf blade area was desirable meaning that plants are more resistant to transplant shock by having less leaf thickness (Masson *et al.* 1991).

2-8. Harvest index and yield formation

Harvest index (HI), a crop-specific fraction of dry mass of harvested component divided by total shoot dry mass, is used to “quantify the yield of a crop species versus the total amount of biomass that has been produced in agriculture” (Blum 2011; ASPS 2018). A higher HI of a crop species is favoured by plant breeders because of the successful plant reproduction and yield, which means the well-functioned assimilate partitioning towards reproduction (Blum 2011).

Harvest Index is a useful tool in the current crop improvement strategy and varies in different crops. For example, the HI values range between 0.4 and 0.6 (kg/kg) for modern varieties of most intensively cultivated grain crops (Hay 1995). This has been exponentially growing due to breeding selection over a century as shown in Figure 2-2 (Evans 1993).

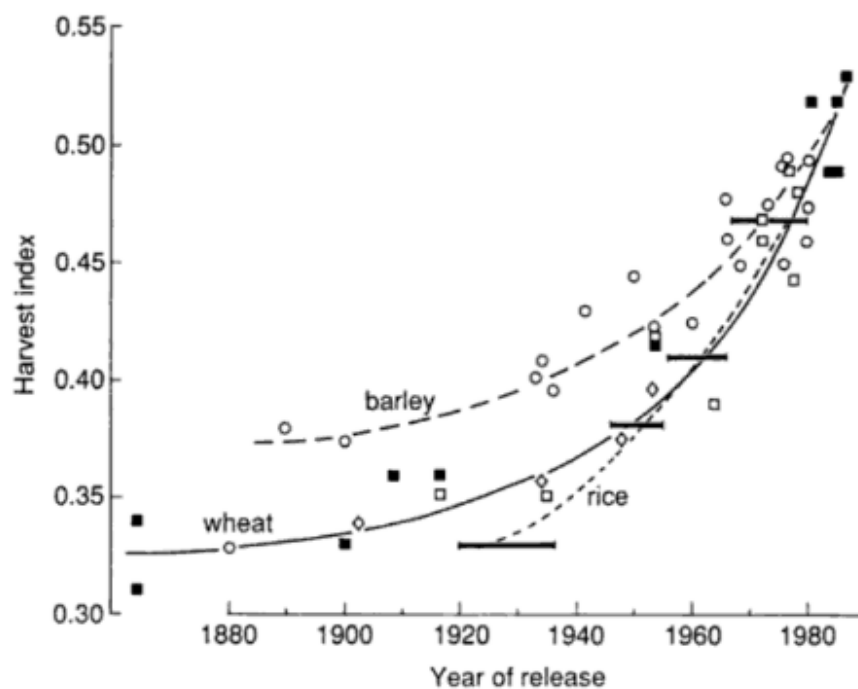


Figure 2-2 Changes of Harvest Index of wheat, barley and rice varieties over a century, adapted from Evans (1993).

As for lettuce, the Harvest Index is calculated differently by the edible parts of plants. The number of leaves is used for non-heading lettuce, such as romaine/cos lettuce whereas maturity of iceberg lettuce is based on size and head compactness (Gil *et al.* 2012). The maturity indicators varied for different goals of use in the fresh-cut industry. For instance, head weight is important for quality assessment for raw material, whereas leaf length and petiole length are crucial for quality control of baby and mature leaves in processed products (Gil *et al.* 2012).

2-9. Potential diseases

Lettuce biomass production is limited by disease susceptibility and unfavourable conditions. Over 75 lettuce disorders caused by diverse pathogens have been described, and the bulk of them are fungi and viruses (Raid 2004). About twenty fungi and oomycetes have reported causing serious problems and at least twenty viruses have been found on lettuce. Potential fungal diseases include anthracnose *Microdochium panattonianum* (Berl.), bottom rot *hanatephorus cucumeris* (A. B. Frank) Donk. (more well-known as *Rhizoctonia solani* Kuhn.), Cercospora leaf spot *Cercospora longissima* Cugini ex Traversonon Cooke & Ellis, nom. illeg., downy mildew *Bremia lactucae* Regel (Oomycete), drop *Sclerotinia*, *S. minor* Jagger and *S. sclerotiorum* (Lib.) de Bary, grey mould *Botrytis cinerea* Pers.:Fr., Septoria leaf Spot *Septoria lactucae* Pass., and southern blight *Sclerotium rolfsii* Sacc. (anamorph) *Athelia rolfsii* Curzi (teleomorph) (Raid 2004). Prevalent viral diseases are beet western yellows virus (BWYV), lettuce big-vein virus (LBVV), which may be the most ubiquitous lettuce disease that there are no known control measures at present, lettuce necrotic yellows (LNYV), which was firstly identified in Australia by Stubbs and Grogan (1963), lettuce mosaic potyvirus (LMV) *etc.*

3. MATERIALS AND METHODS

3-1. Study site

The field trials studying iceberg lettuce were located at Koala Farms (27°32'05.6"S, 152°20'55.9"E) in the Lockyer Valley Region, Queensland (Figure 3-1). The soil type at this farm is classed as a black Vertosol [VE-AE], which has a typical clayey texture with shrink-swell properties, based on the Australian Soils Classification system (Isbell 2016). The Lockyer Valley is a Subtropical environment (810.4 mm precipitation annually) with warm humid summers (mean maximum and minimum temperatures are 31.6°C and 19.3°C with precipitation average 120.2mm in January) and mild dry winters (mean maximum and minimum temperatures are 20.7°C and 6.2 °C with precipitation average 26.1mm in July) (BOM 2001; ABCB 2015). Over the whole course of the lettuce development, Arable Mark 2[®] sensor (San Francisco, CA, USA) (www.arable.com/) recorded the weather data and a time-lapse camera (WingScape[®] or Swift Enduro[®] 4G) (see Plate 3-1) took the image of lettuce growth every two hours during the day.



Plate 3-1 Setting up the two devices in the paddock (top: time-lapse camera; bottom: Arable Mark 2 sensor).

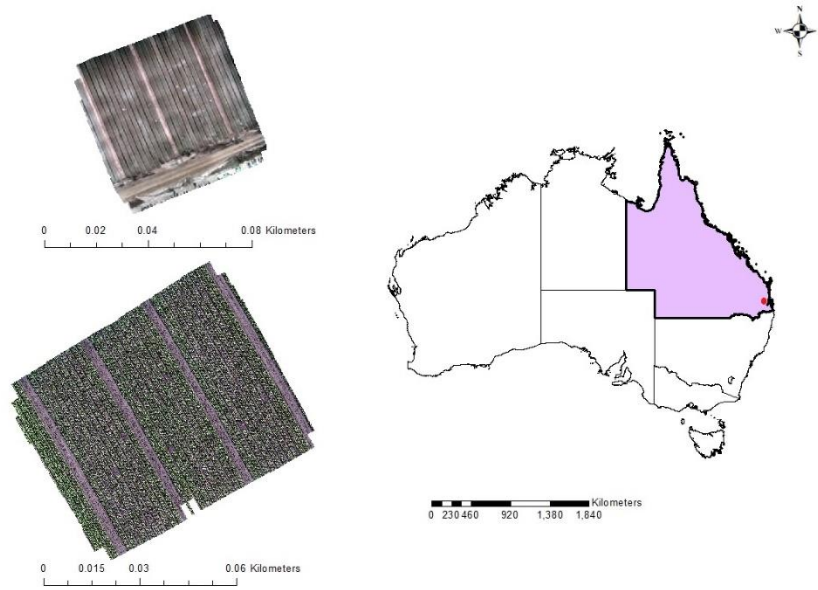


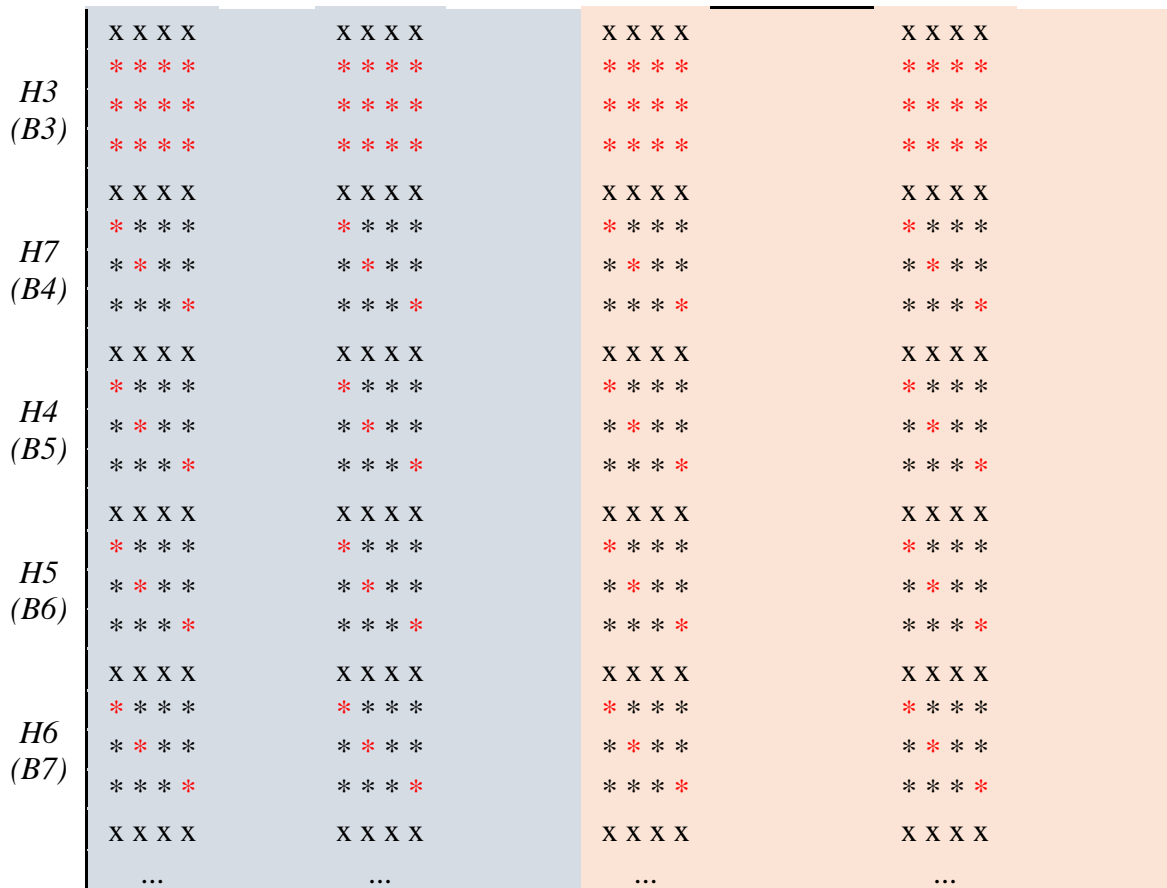
Figure 3-1 Site location with paddock sizes for two growing seasons.

3-2. Cultivars, experimental design and layout scheme

Iceberg lettuce (cultivar: Vintage Crop) was transplanted on the 9th April 2020 (Transplant date) into bays, 4 plants wide and several hundred long. Similarly, in another paddock, iceberg lettuce (cultivar: Carabine) was transplanted on the 19th May 2020. In each season, there were four sampling blocks in each of the 4 bays. In each block/bay, 12 plants were harvested down the field, leaving a border of one plant across the bay between each harvest (Table 3-1).

Table 3-1 Experimental layout * lettuce samples harvested; red highlighted: lettuce samples dehydrated.

Bed No.	Bay 1				Bay 2			
	1	2~5	6	7~10	11	12~15	16	17~20
	∴		∴		∴		∴	
H1 (B1)	X X X X		X X X X		X X X X		X X X X	
	* * * *		* * * *		* * * *		* * * *	
	* * * *		* * * *		* * * *		* * * *	
	* * * *		* * * *		* * * *		* * * *	
H2 (B2)	X X X X		X X X X		X X X X		X X X X	
	* * * *		* * * *		* * * *		* * * *	
	* * * *		* * * *		* * * *		* * * *	
	* * * *		* * * *		* * * *		* * * *	



3-3. Destructive sampling

Above-ground biomass accumulation of lettuce in each plot was assessed through destructive sampling. At each harvest, a total of 48 plants (*ca.* 12 plants from each of 4 blocks) were cut at ground level. In the laboratory, each plant was weighed fresh, and at first three harvest events, all plants were dehydrated into four separate paper bags by the plot and weighed, and for the rest of harvest events, 3 of 12 plants (*ie* 1st, 6th and 12th, see analogised red dots in Table 3-1) were selected to be dried and weighed. At the final harvest, each of the 48 plants was also trimmed according to market practice and weighed, and then also trimmed to the core, and weighed. In this harvest, 3 plants per block were also dried after the two trimming processes. Figure 3-2 shows the flow diagram of the procedures of destructive sampling.

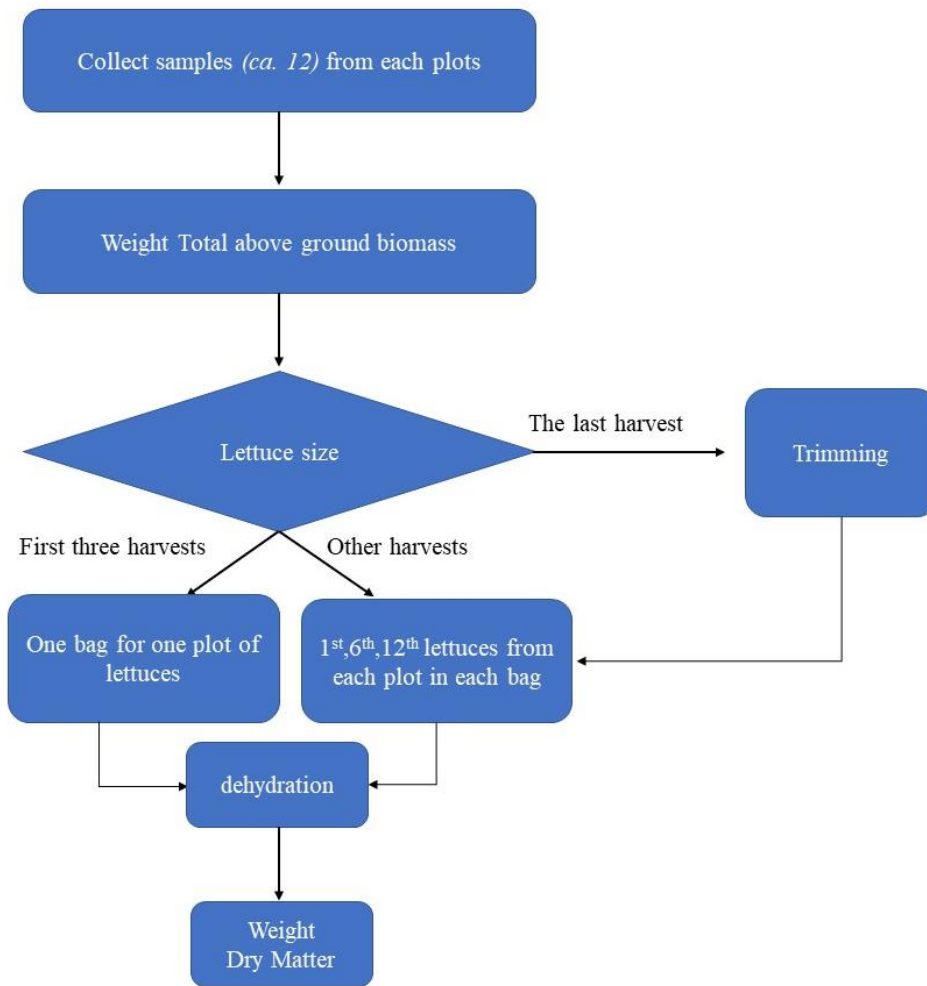


Figure 3-2 Flow diagram outlining the destructive sampling process.

3-4. Marketable Harvest Index, Water Content, Light Use Efficiency

Marketable harvest index (MHI, g/g) was calculated by dividing market-standard trimmed fresh biomass (g) by the total biomass (g), whilst the water content (WC) was calculated by the following equation:

$$WC = 1 - \frac{\text{Dry Matter}}{\text{Total Biomass}}$$

Equation 3-1

Crop biomass is the result of solar energy accumulation utilised and stored by plant cells, and in this process, an integral function can be simplified into the following function, and LUE is the conversion ratio and slope of this function:

$$CBD = DW_n - DW_0 = LUE \times \sum_0^n (Rad_n \times fINT)$$

Equation 3-2

3-5. Thermal time

Thermal time (TT, °Cd), also known as growing degree days (GDD), works in daily fluctuating temperature as in stable temperature in a temperature-dependent way because the temperature is the overriding effect on most physiological processes, particularly when comparing multiple courses of days and experiments. (Sadok *et al.* 2007). The following equation was posed by (Gallagher 1979); McMaster and Wilhelm (1997) for each two-time series analyses.

$$TT_{sum} = \sum_{i=1}^{i=n} \left[\left(\frac{T_{max} + T_{min}}{2} \right) - T_b \right] = \sum_{i=1}^{i=n} (T_{avg} - T_b)$$

Equation 3-3

Conditions:

(1) if T_{max} or $T_{min} < T_b$, T_{max} or $T_{min} = T_b$

(2) if $T_{avg} < T_b$, $T_{avg} = T_b$, $TT=0$

(3) if T_{max} or $T_{min} > T_{opt}$, T_{max} or $T_{min} = T_{opt}$

In this equation, T_b is an empirically derived base temperature that drops at the zero growth of crops. T_{max} and T_{min} are maximum and minimum daily temperature respectively. n is the number of days of temperature observation. For lettuce, according to (Wheeler *et al.* 1993b), T_b is 0 °C (Wurr & Fellows 1984) and T_{opt} is 25 °C, derived from (Lorenz & Wiebe 1980). Others have used 4°C and 6°C as base temperatures (Gray & Morris 1978; Kristensen *et al.* 1987) and 35°C as an optimum temperature (Bensink 1971; Wheeler *et al.* 1993a).

3-6. RGB imagery analysis

In order to produce high-quality RGB images, DJI Phantom 4 Advanced[®] (Shenzhen, China) (www.dji.com/) (see Plate 3-2) was used to take images at three different altitudes of 10m, 20m and 40m. The flight path was designed to be flown across the target plots in a gridded pattern exported from Pix4D[®] (Prilly, Switzerland) (www.pix4d.com) (See Plate 3-3). The drone was set up to have a 1/800 second shutter speed.



Plate 3-2 Phantom 4 Advanced with an RGB camera sitting on a GCP mat.

The accurate georectification of RGB images, four ground control points (GCPs) were placed toward the top of the trial. The GCPs were black-white colour mats painted with the plot number, which can be easily identified in the flight images. Each centre of GCPs was coordinated by Propeller AeroPoints[®] (Surry Hills, Australia) (www.propelleraero.com/). The AeroPoints were placed on the top of each GCPs for around one hour receiving satellite signals to have very precise georeferencing locations producing Universal Transverse Mercator (UTM) coordinate system easting (m) and northing (m) coordinates, along with orthometric height (m) to a 2cm accuracy. The conversion between UTM and Geographic Coordinate System (GCS) can be achieved by R.

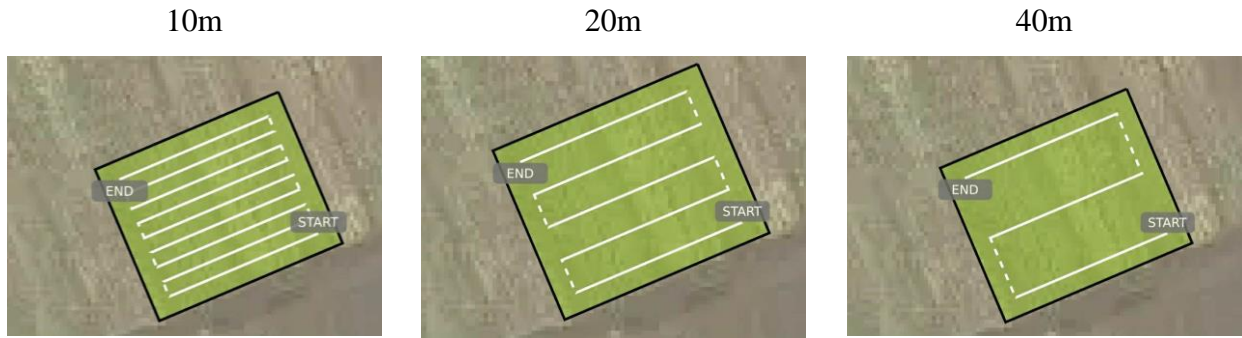


Plate 3-3 Flights path in 10m, 20m and 40m respectively.

3-7. Ground Sample Distance

Ground Sample Distance (GSD, cm/px) is an important parameter used as the formulation of the specifications for photogrammetric flight missions, replacing traditionally-used concept: photo scale (Felipe-García *et al.* 2012). GSD is defined as the “distance between pixel centre from a digital photo measured in millimetres on the ground”(Figure 3-3) (González-Quiñones *et al.* 2018). It could be calculated by two methods and GSD_w (worst case scenario) was adopted in this project (Propeller Aero 2018).

$$GSD_w = \frac{FlightHeight \times SensorWidth}{FocalLength \times ImageWidth}$$

or

$$GSD_h = \frac{FlightHeight \times SensorHeight}{FocalLength \times ImageHeight}$$

Equation 3-4

Table 3-2 Specifications of DJI Phantom 4 Advanced were used to calculated GSD, collected from (DJI n.d.).

Specifications	Parameters
Sensor Width (mm)	13.2
Senor Height (mm)	8.8
Focal Length (mm)	8.8
Image Width (pixels)	5472
Image Height (pixels)	3648

GSD_w for 20m \approx 0.4cm/px

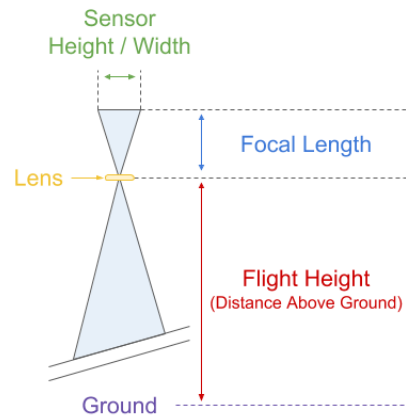


Figure 3-3 Visual representation of calculating GSD, adopted from Propeller Aero (2018).

3-8. Image processing

Images were processed by either PhenoCopter (CSIRO Agriculture and Forestry Flagship, Brisbane, Australia) (phenocopter.csiro.au/) or Agisoft Metashape Pro (St Petersburg, Russia). In order to produce orthomosaic images for each flight, the following steps are involved in this process: importing images, aligning photos, building a dense cloud, building a mesh and finally producing an orthomosaic image (Figure 3-4).

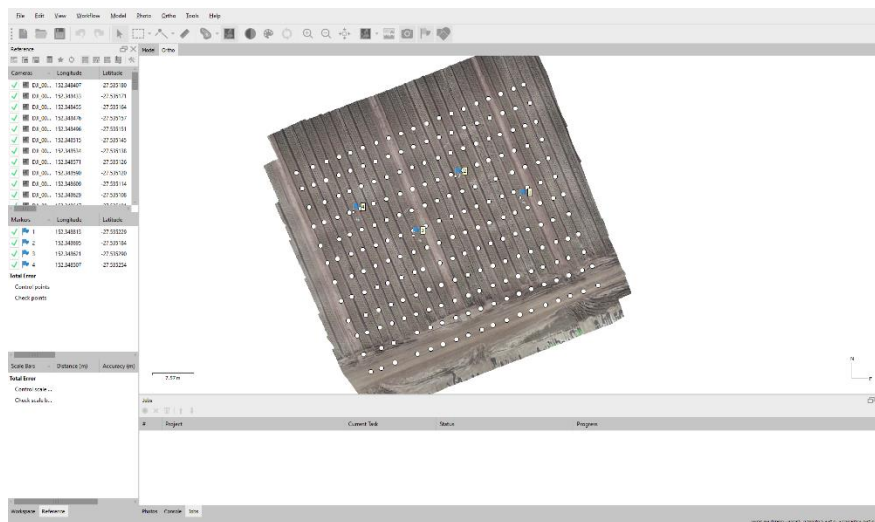
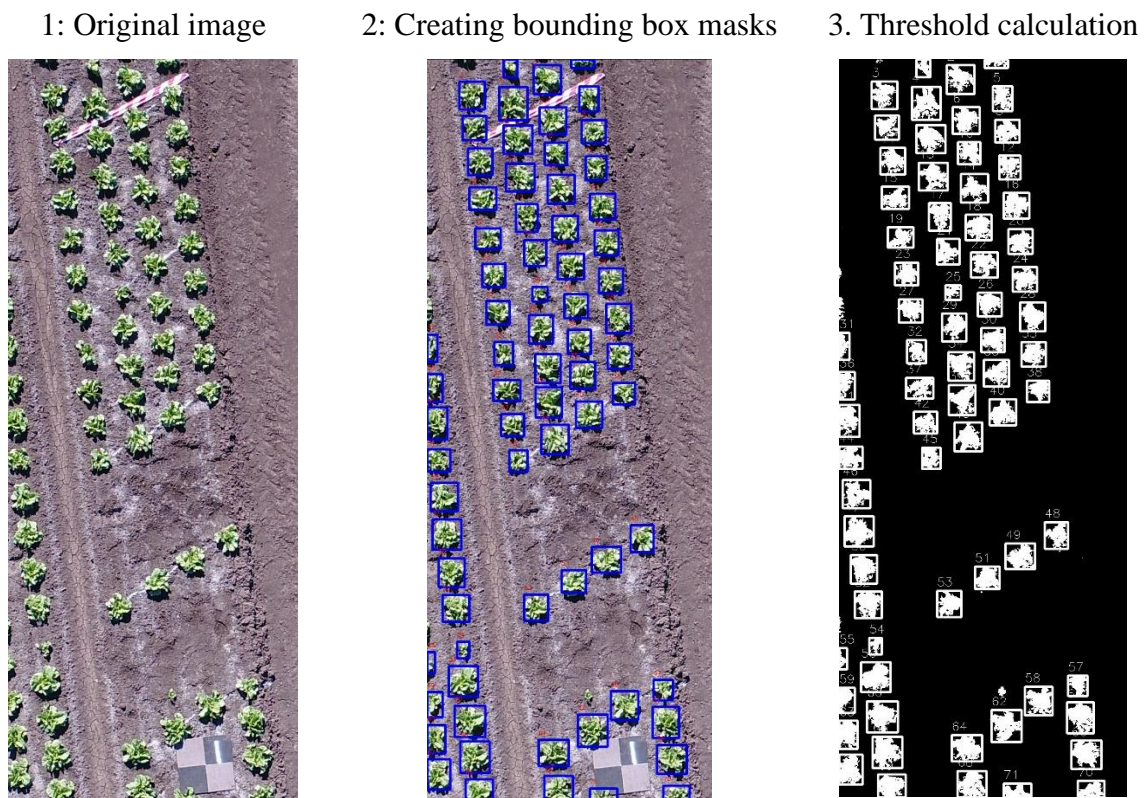


Figure 3-4 An orthomosaic image of a flight with GCPs and image points was produced in Agisoft.

3-9. Image feature extraction

A Python script written by James (2020) was used to extract the lettuce area in pixel counts by differentiating soil and plant colours in each pixel. The green threshold was set as from [23, 23, 31] to [90, 255, 255] in HSV (Hue, Saturation, Value) format to segment groups of pixels by a decision tree. If the surrounding pixels were located within the range of thresholding HSV values, the computer was able to draw bounding box masks around each group [Step 2 in Table 3-3], and each pixel was counted within the groups [Step 3 in Table 3-3]. Thus, plant area data were collected from 20m flight original images saved in CSV files. Table 3-3 is an example using this Python script.

Table 3-3 Three steps in image feature extraction



3-10. Biovolume estimation

The plant biovolume data were collected from 20m flight orthomosaic images set by the medium quality of mesh 3D model. The polygons of individual lettuce were drawn in Agisoft and formed a base plane which was set as “best-fit plane” in each polygon. The software could estimate the volume above the plane automatically (See Figure 3-5).

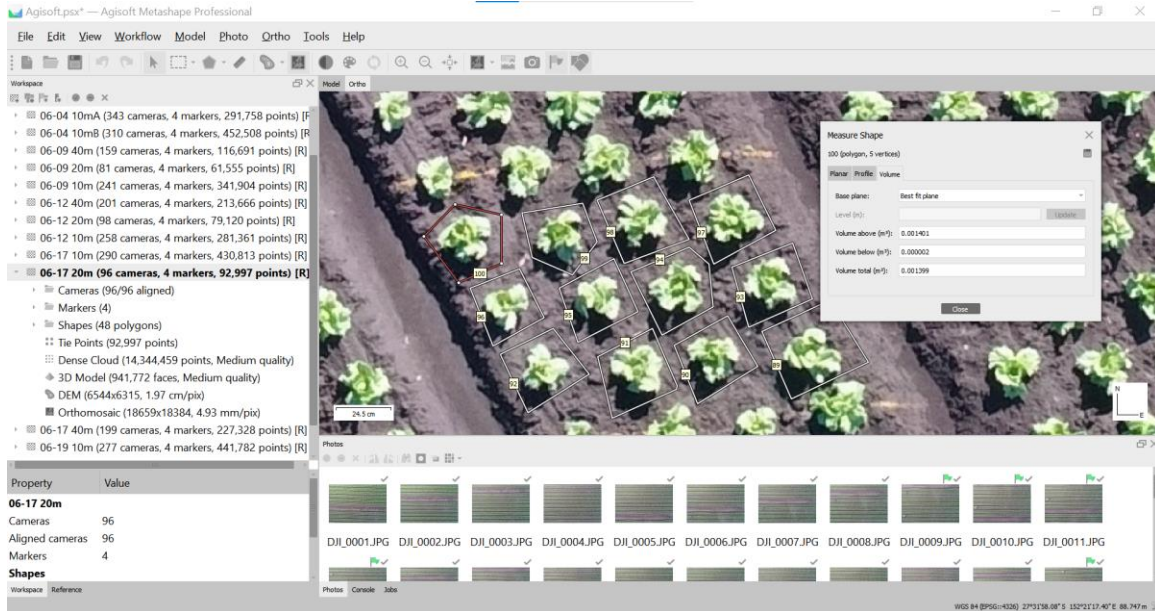


Figure 3-5 Calculating volumes lettuce by drawing polygons (bounding boxes) around each individual.

3-11. Lettuce biomass simulation

The weather data for 2001 to 2020 for the data from the Bureau of Meteorology (2020) (Site ID: 040082) were utilised for example simulations in a simple lettuce model. For the same transplant dates each year (9 April, 19 May), daily thermal time was calculated using $T_b = 7^\circ\text{C}$. For the two experiments in 2020, the observed thermal time to harvest (TTFH) was calculated from the calendar date of harvest. This TTFH was set as a target thermal time for the two sample dates, and the calendar date of harvest was simulated for 20 years. The models were applied for four different periods of harvesting time (at 40, 50, 60, 70 DAT)

3-12. Statistical analysis

All statistical analysis and plotting in this project were performed in RStudio with the help of multiple R packages (“tidyverse”, “reshape2”, “tidyr”, “ggpmisc”, “RColorBrewer”, “lme4”, “gghighlight”, “Rmisc”, “segmented”, “nlraa”, “ggrepel”, “nlme”, “scales”, “rgdal”, “sp”, “maptools”, “data.table”, “proj4”, “dtplyr”, “data.table”, “lubridate”, “ggpubr” *etc.*). Sigmoid curves were fitted into fresh biomass, water content and dry weight accumulation against thermal time by logistic regression. Piecewise functions with exponential curves and constant y-values were applied to the fraction of intercepted radiation against thermal time. and plant biovolume against thermal time was fitted with exponential curves as well. Intercepted solar radiation was plotted against thermal time by expo-linear growth model. The interactions amongst other key factors were fitted with linear regressions. The outputs of the coefficient of determination (adjusted R^2 for linear regression and Quasi- R^2 for logistic regression) served to justify different model outputs across different days after transplanting (DATs), cumulative thermal time and seasons in linear models. The expo-linear growth model was proposed by Goudriaan and Monteith (1990) to compare the interception radiation.

4. RESULTS

4-1. Environmental conditions

Throughout the two growing seasons (Season 1, transplant date: 9 April; Season 2, transplant date: 19 May), a total of rainfall for each season was 11 mm and 51 mm, respectively (Figure 4-1 and Figure 4-2). The cumulative incident solar radiation (*short-wave solar radiation*: 0.3-3.0 mm) received during these two seasons was plotted against the cumulative thermal time in Figure 4-3. In Season 1, the average maximum and minimum temperatures were 26.6°C and 11.3°C, whereas, in Season 2, the values had dropped to 21.9°C and 8.6°C. Lower winter temperature prolonged maturity, but a similar amount of incident solar radiation cumulatively was received (666 v. 675 °Cd in Figure 4-3). In those figures, the detailed weather from the paddocks received by Arable Mark sensor started from the thermal time indicated by the vertical lines. Before this date, data from the Bureau of Meteorology (2020) (Site ID: 040082) were adopted.

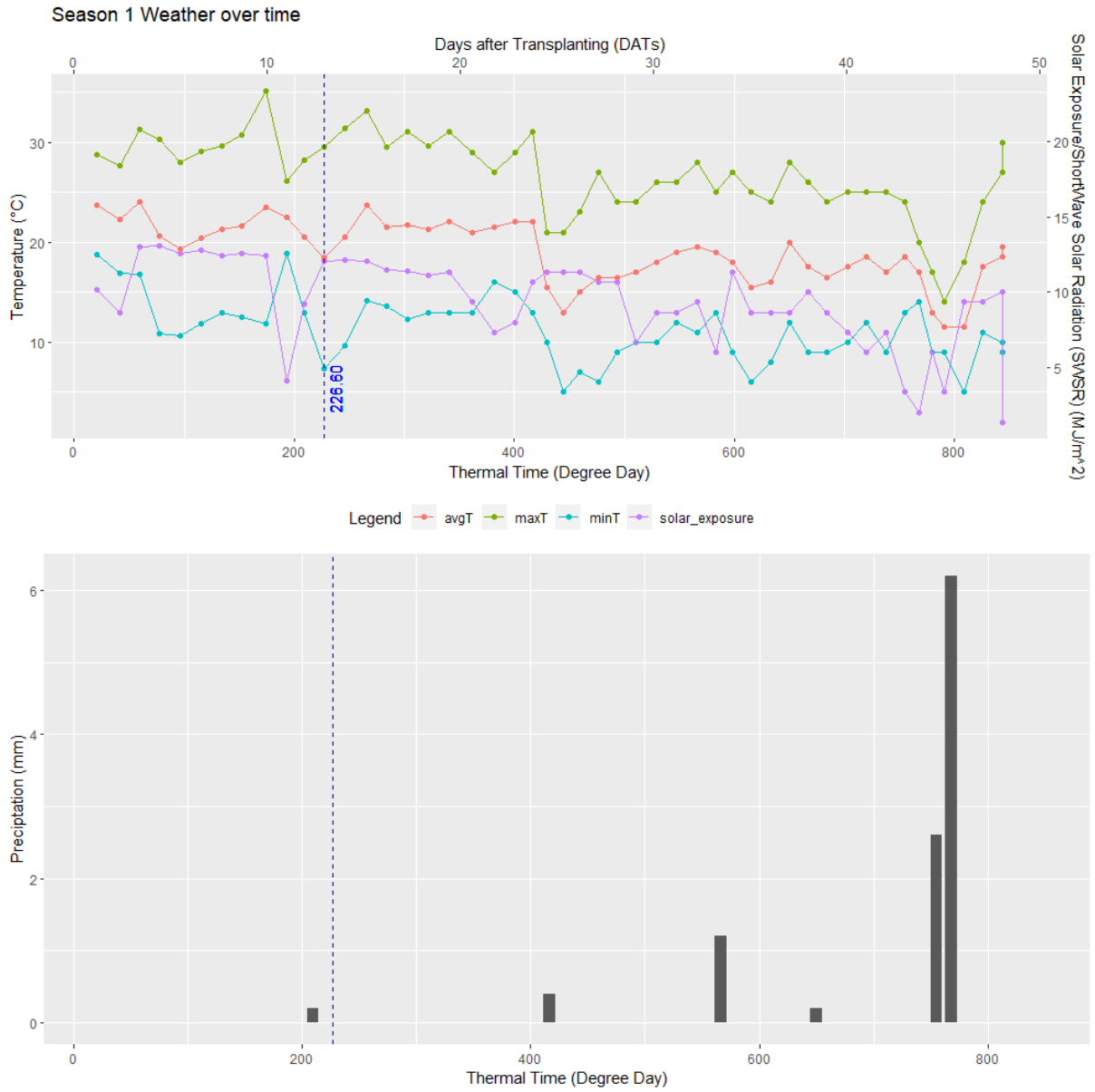


Figure 4-1 Seasonal weather conditions of Season 1 including daily minimum and maximum temperature, solar radiation along with precipitation over thermal time.

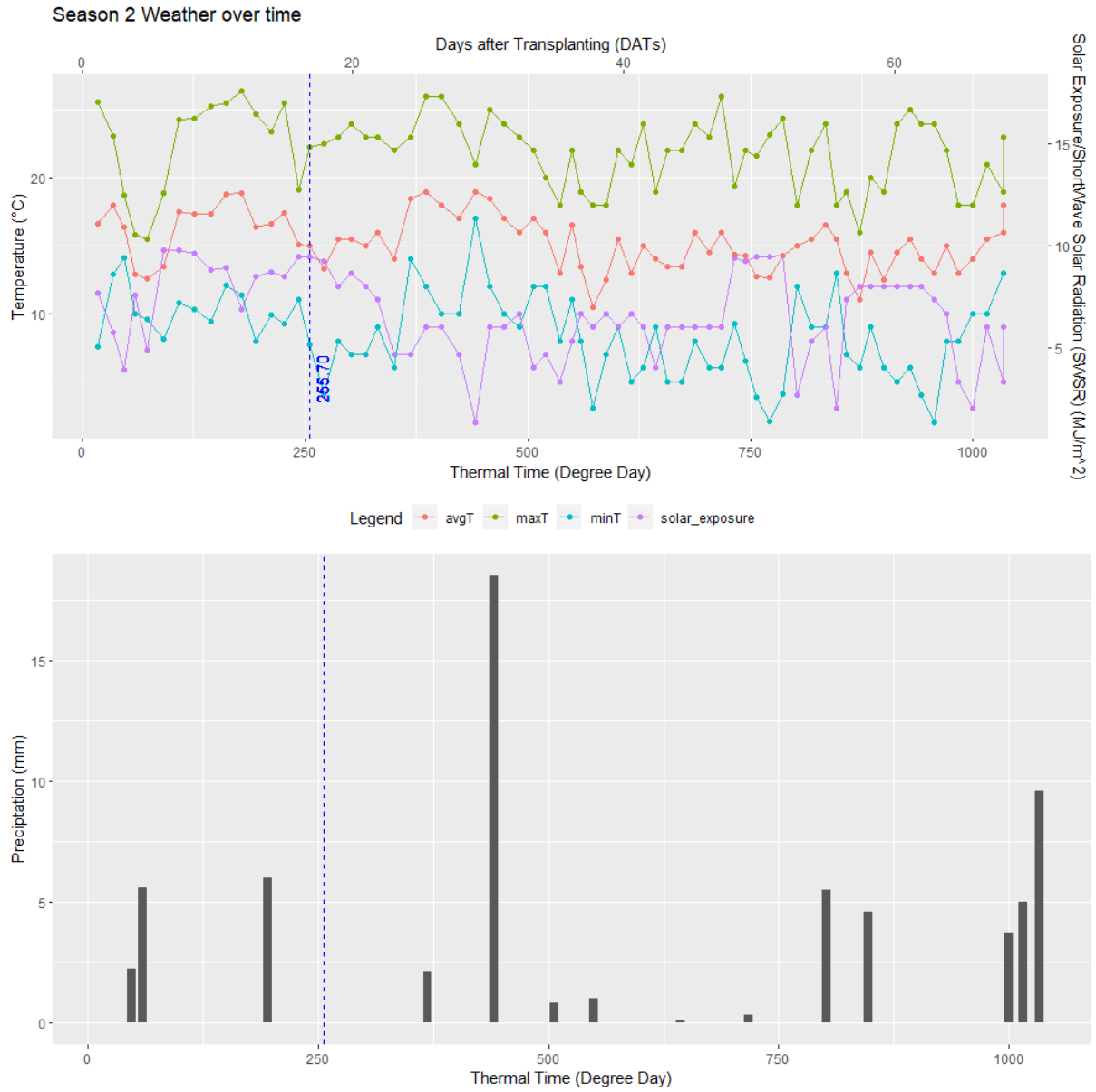


Figure 4-2 Seasonal weather conditions of Season 2 including daily minimum and maximum temperature, solar radiation along with precipitation over thermal time.

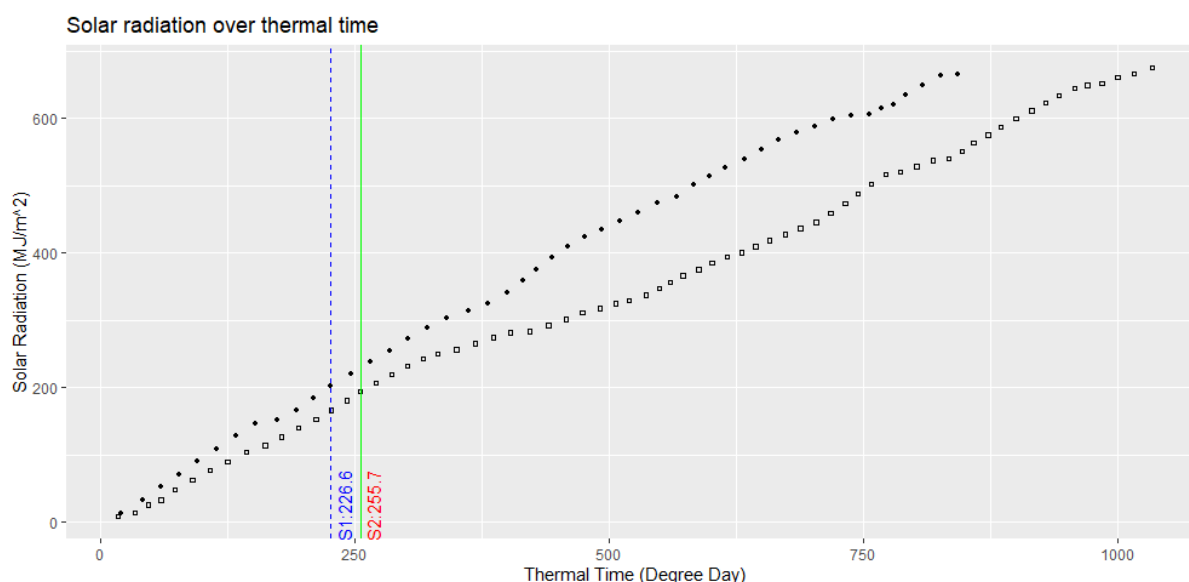


Figure 4-3 Cumulative thermal time and cumulative solar radiation for • Season 1 and ◻ Season 2.

4-2. Crop growth models over thermal time

Crop growth models can be characterised by plant biomass, the fraction of intercepted radiation, biovolume and dry matter throughout thermal time. Table 4-1 summarised the models between key plant physiological traits against cumulative thermal time.

Table 4-1 Fitted curves for crop growth by fresh biomass (g/plant), the fraction of intercepted radiation ($fINT$, -), biovolume (m^3/m^2), dry matter (g/plant) and water content (per plant) against Cumulative Thermal Time ($^{\circ}Cd$).

Response Variables	Explanatory Variable(s)	S1	S2
Fresh Biomass	Cumulative Thermal Time	1154	2385.10
$fINT$		$1 + e^{\left[-\frac{1}{96.44}(TT-463.998)\right]}$ $e^{0.005951445TT-3.625329}$ $(0 < TT < 609.151^{\circ}Cd)$ $1.0 (TT > 609.151^{\circ}Cd)$	$1 + e^{\left[-\frac{1}{154.46}(TT-761.14)\right]}$ $e^{0.007155303TT-4.609029}$ $(0 < TT < 644.142^{\circ}Cd)$ $1.0 (TT > 644.142^{\circ}Cd)$
Biovolume		$e^{0.006245311TT-4.872403}$	$e^{0.005341311TT-5.591687}$

Dry Matter	$\frac{35.843}{1 + e^{\left[-\frac{1}{98.183}(TT-380.120)\right]}}$	$\frac{44.579}{1 + e^{\left[-\frac{1}{93.338}(TT-467.529)\right]}}$
Water Content	$\frac{0.9601}{1 + e^{\left[-\frac{1}{181.4}(TT-455.6)\right]}}$	$\frac{0.97412}{1 + e^{\left[-\frac{1}{405.647}(TT-875.08552)\right]}}$

Plant biomass (*Quasi-R² S1:0.92; S2:0.91*), water content (*Quasi-R² S1:0.91; S2:0.82*) and dry weight (*Quasi-R² S1:0.97; S2:0.96*) against cumulative thermal time were fitted with logistic regression. fINT and biovolume against cumulative thermal time were fitted with exponential curves.

4-2-1. Plant biomass accumulation

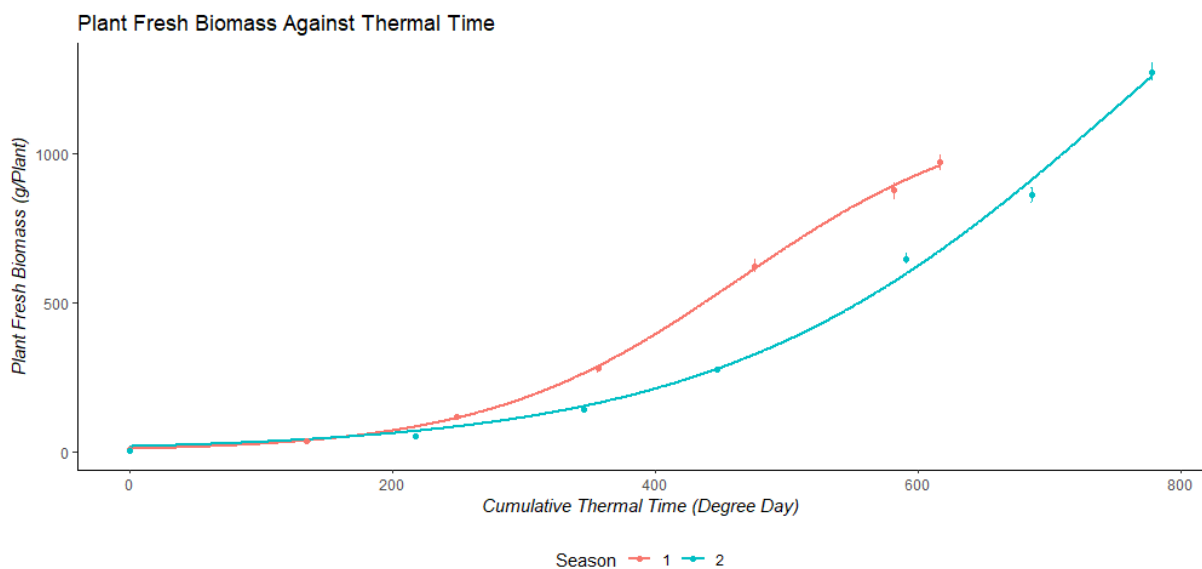


Figure 4-4 Plant Fresh Biomass was plotted against Cumulative Thermal Time in contrasting seasons fitted with logistic regression. The relative cumulative thermal time started from the first harvest.

4-2-2. Fraction of intercepted radiation

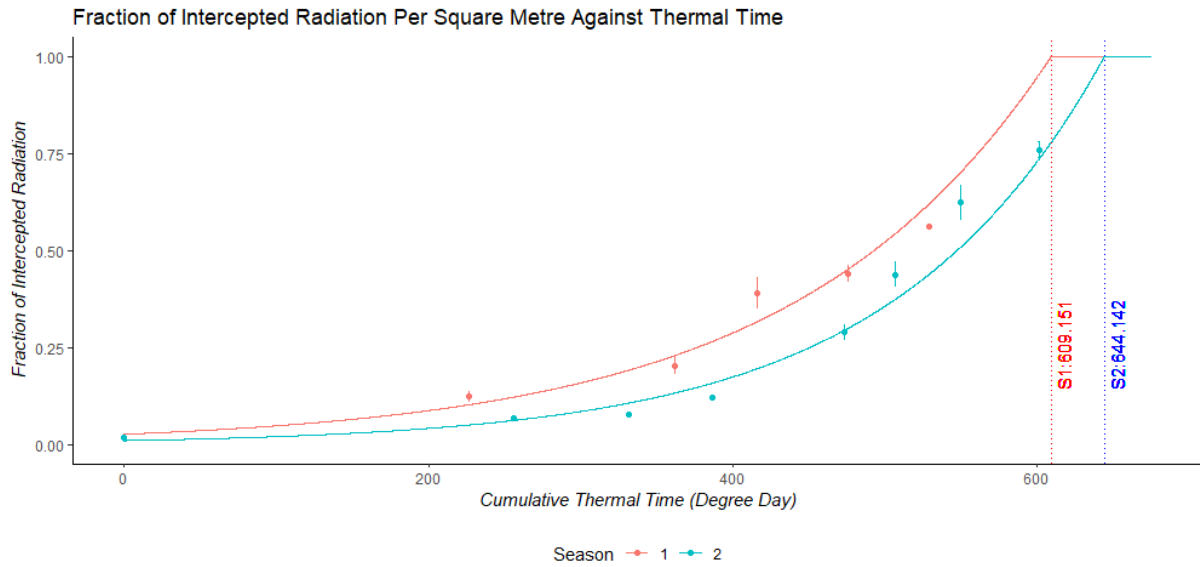


Figure 4-5 Fraction of Intercepted Radiation was plotted against Cumulative Thermal Time in contrasting seasons fitted with exponential curves started from the dates of transplanting. (maximum fraction of intercepted radiation = 1)

4-2-3. Plant volume expansion

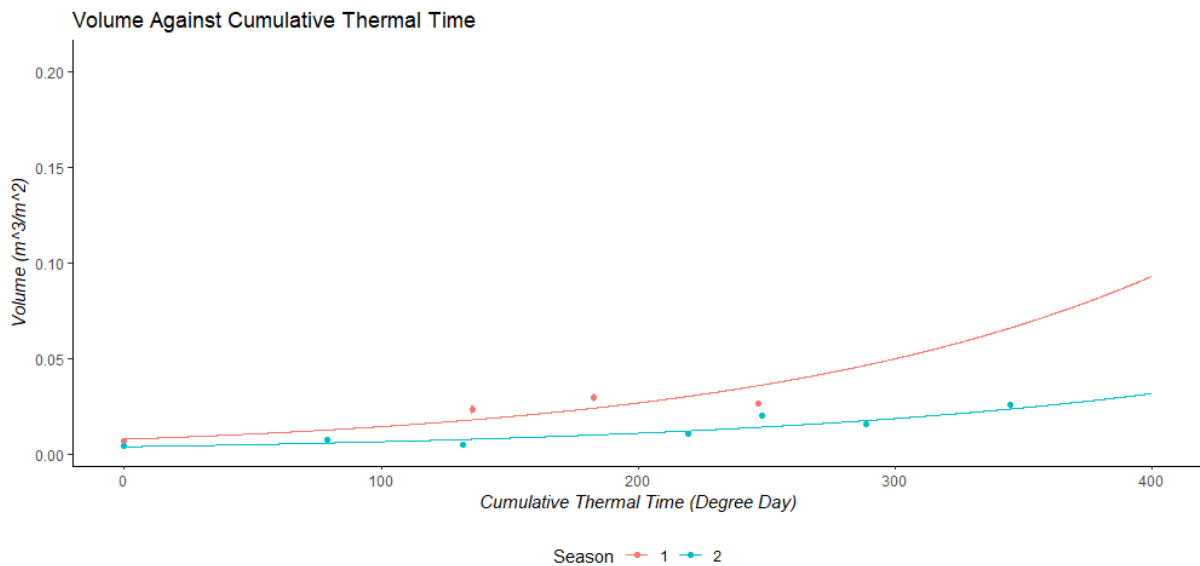


Figure 4-6 Plant Volume was plotted against Cumulative Thermal Time in contrasting seasons fitted with exponential curves started from the first harvest.

4-2-4. Plant dry matter accumulation

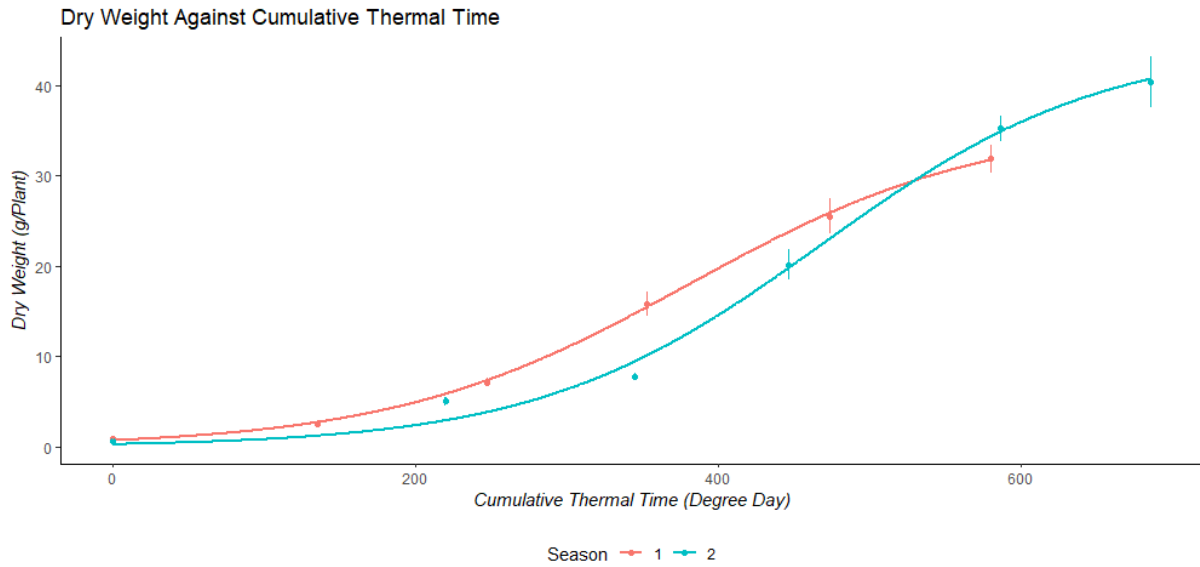


Figure 4-7 Plant Dry Weight was plotted against Cumulative Thermal Time in contrasting seasons fitted with logistic regression started from the first harvest.

4-2-5. Water content

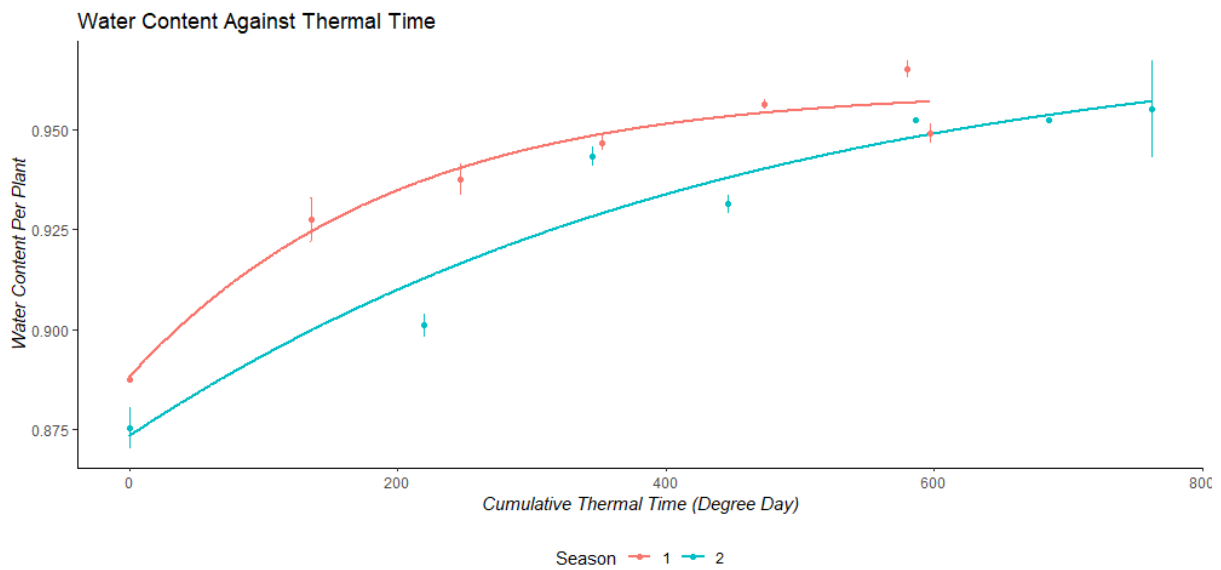


Figure 4-8 Water Content was plotted against Cumulative Thermal Time in contrasting seasons fitted with logistic regression started from the first harvest.

4-3. Correlations between plant area and plant biomass

4-3-1. Real-Time models

Fresh biomass of individual lettuce in harvest blocks was plotted at the day of flight against the area of the same plants that had been harvested. Figure 4-9 and Figure 4-10 illustrated the relationships between plant area and biomass in the first three harvests fitted with linear regression. The correlation of determination for 1st harvest in Season 2 (*adjusted R*²:0.67) has much higher than in Season 1 (*adjusted R*²:0.25); whereas for 3rd harvest, Season 1 (*adjusted R*²:0.79) has higher than in Season 2 (*adjusted R*²:0.46).

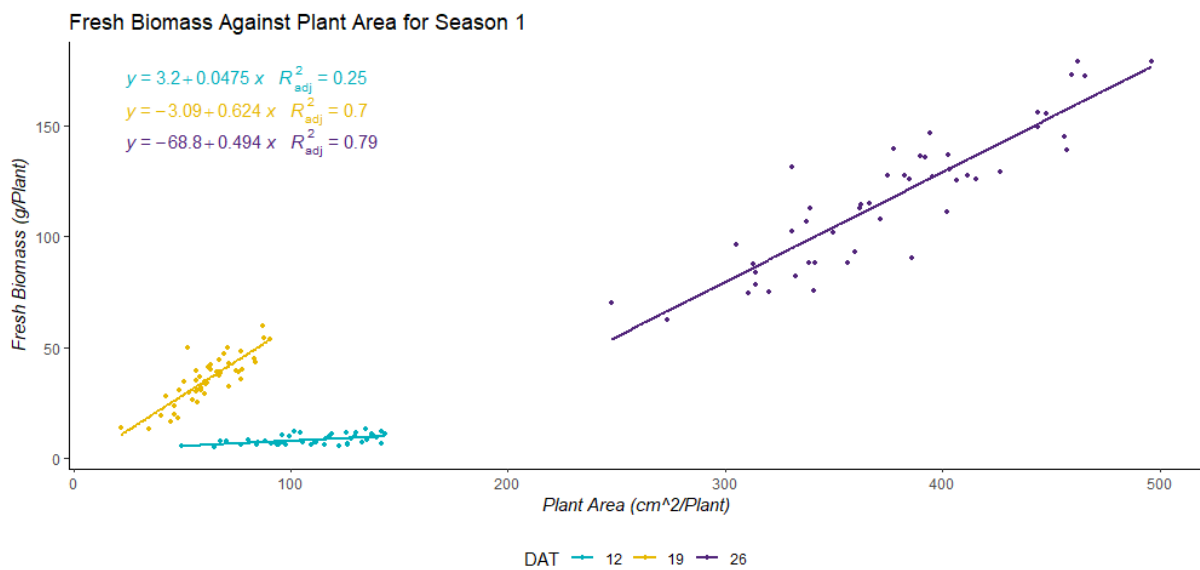


Figure 4-9 The correlations between fresh biomass of harvest plots from each harvest and plant area of harvest plots from each flight in Season 1 fitted with linear regression.

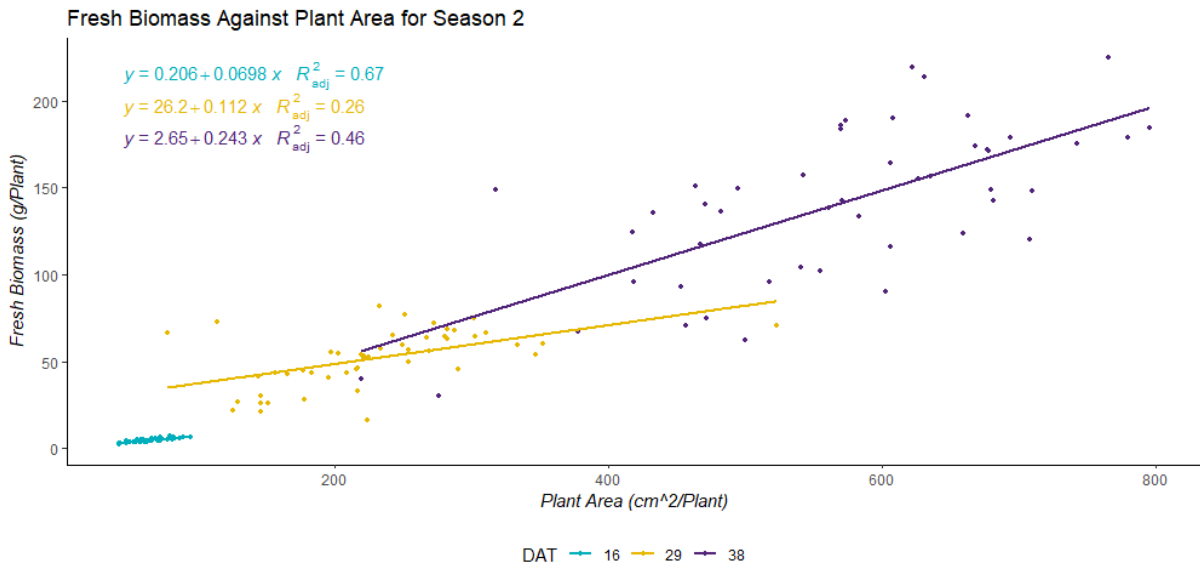


Figure 4-10 The correlations between fresh biomass of harvest plots from each harvest and plant area of harvest plots from each flight in Season 2 fitted with linear regression.

4-3-2. Prediction models

We compared data from successive flight dates with fresh biomass of the 48 plants harvested at the final date. Table 4-2 summarised the prediction models fitted with linear regression (see Figure 4-12 for Season 1 and Figure 4-13 for Season 2) between fresh biomass from the final harvest [H7 Block] and plant area of final harvest plots [H7 Block] over each flight in term of days after transplanting. Combined with Figure 4-11, it revealed that models from Season 2 are more significant than in Season 1, by comparing the highest peak of adjusted R² values, the models were fitted best around 400 °Cd.

Table 4-2 Summary of models to predict fresh biomass from the final harvest of 48 plants using the estimated plant area of those same plants for each flight date, The cumulative thermal time started from the date of transplanting. • Season 1 harvests; ◻ Season 2 harvests

Seasonality	TT (GDD, °Cd)		Adjusted R ²	
	SI	S2	SI	S2
DATs				
12•	226.60		0.111	

16 [□]	255.70		0.524
19 [•]	361.60	0.348	
21	331.70		0.451
22	416.10	0.417	
24	386.20		0.539
26 [•]	476.10	0.355	
29 [□]	529.10	473.70	0.038
31	506.70		0.451
34	549.70		0.307
38 [□]	601.20		0.234

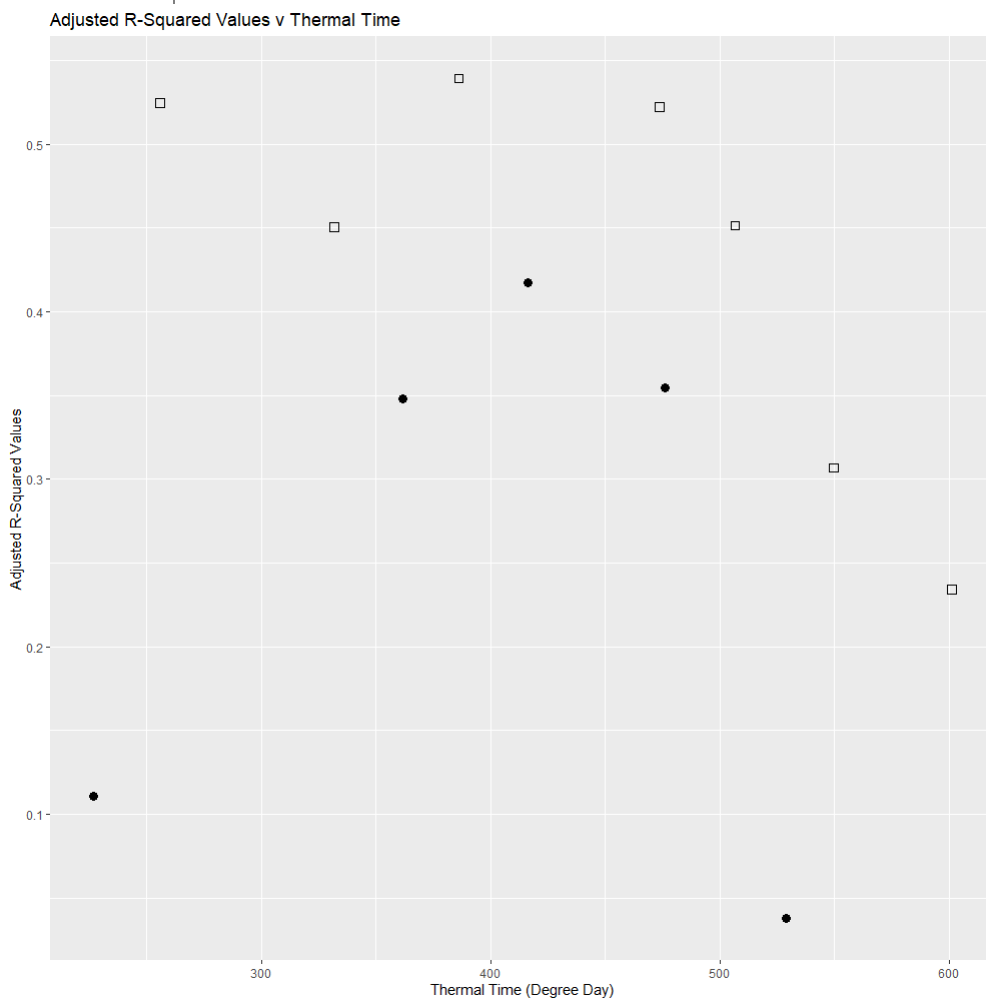


Figure 4-11 Adjusted R-squared values from the above models were plotted against Cumulative Thermal Time. • Season 1; □ Season 2

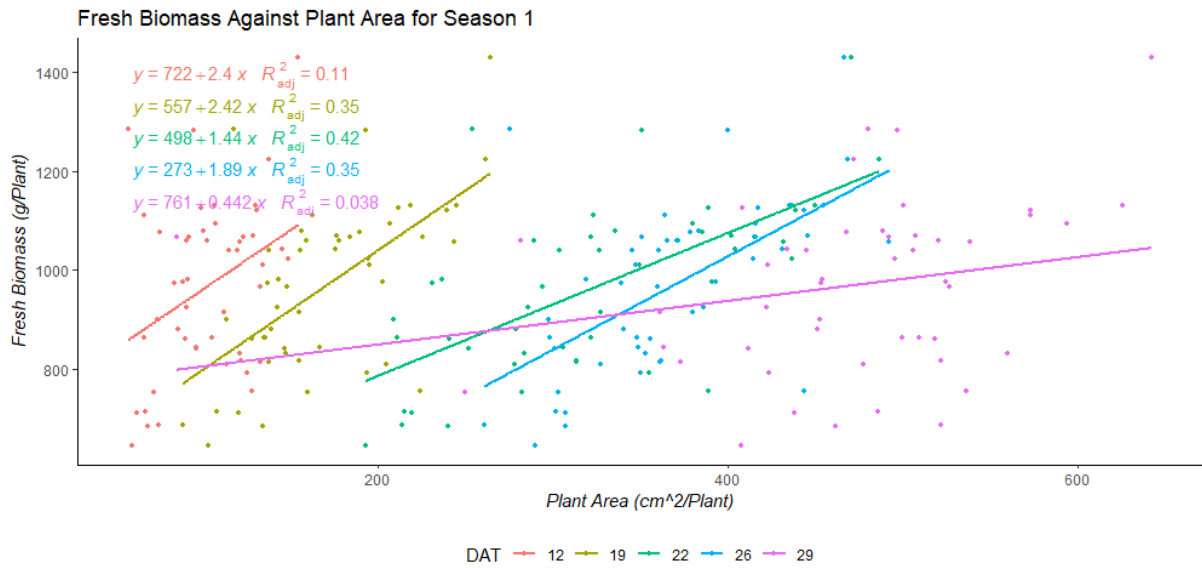


Figure 4-12 Fresh biomass from the final harvest was plotted against plant area of final harvest plots over each flight in Season 1 fitted with linear regression.

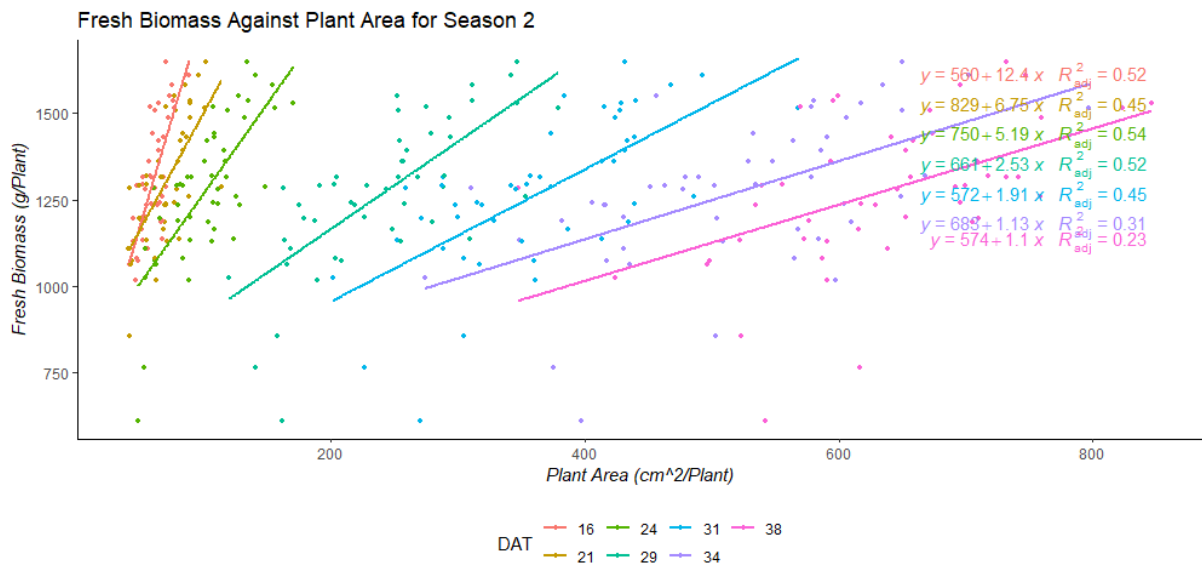


Figure 4-13 Fresh biomass from the final harvest was plotted against the plant area of final harvest plots over each flight in Season 2 fitted with linear regression.

4-4. Correlations between plant biovolume and plant biomass

4-4-1. Real-Time models

Figure 4-14 and Figure 4-15 were plotted to correlate the fresh biomass and biovolume of the same plants at each harvest date. The adjusted R^2 values were not linearly correlated for both Season 1 and Season 2. The strongest adjusted R^2 (0.62) value was found at 601.2 °Cd (DAT: 38) in Season 2.

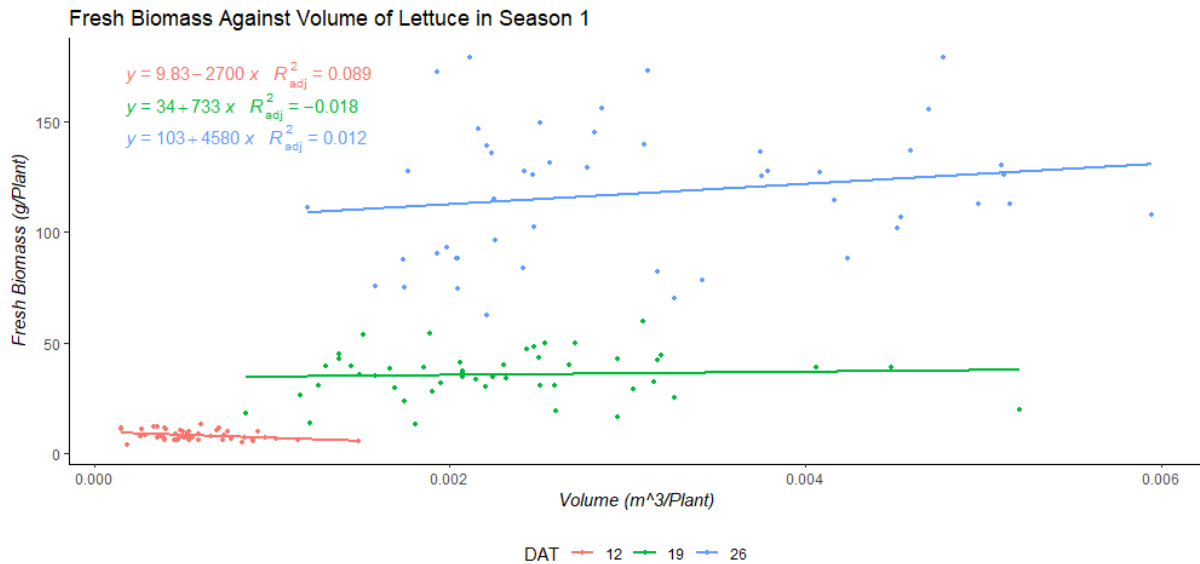


Figure 4-14 The correlations between fresh biomass and plant biovolume of each harvest plots in Season 1 fitted with linear regression.

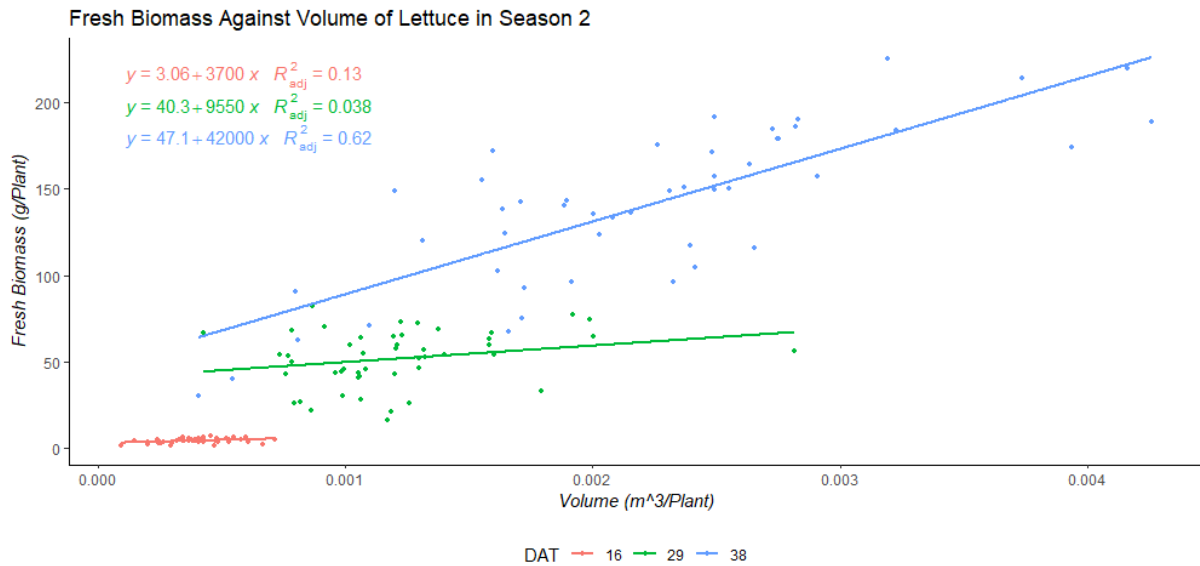


Figure 4-15 The correlations between fresh biomass and plant biovolume of each harvest plots in Season 2 fitted with linear regression.

4-4-2. Prediction models

By measuring biovolume of 48 plants [H7 Block] in reconstructed 3D models at each flight dates, we tried to predict the fresh biomass at the final harvest from biovolume of the same plants at early stages. Figure 4-16 and Figure 4-17 suggested that the best fitted linear model with an adjusted R^2 value of 0.35 was at 416.1 °Cd (DAT: 22) and the adjusted R^2 value of the model dropped to 0.17 in Season 1. In contrast to Season 2, the best-fitted model increasingly reached its adjusted R^2 value peak of 0.59 is at 601.2 °Cd (DAT: 38).

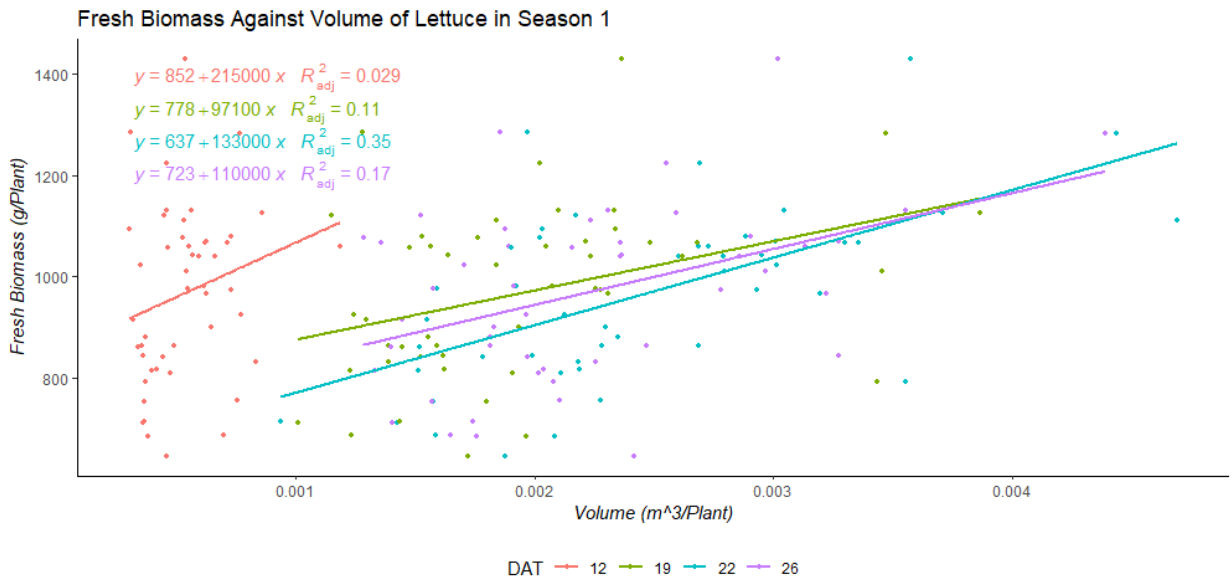


Figure 4-16 The correlations between fresh biomass and plant biovolume of final harvest plots in Season 1 fitted with linear regression.

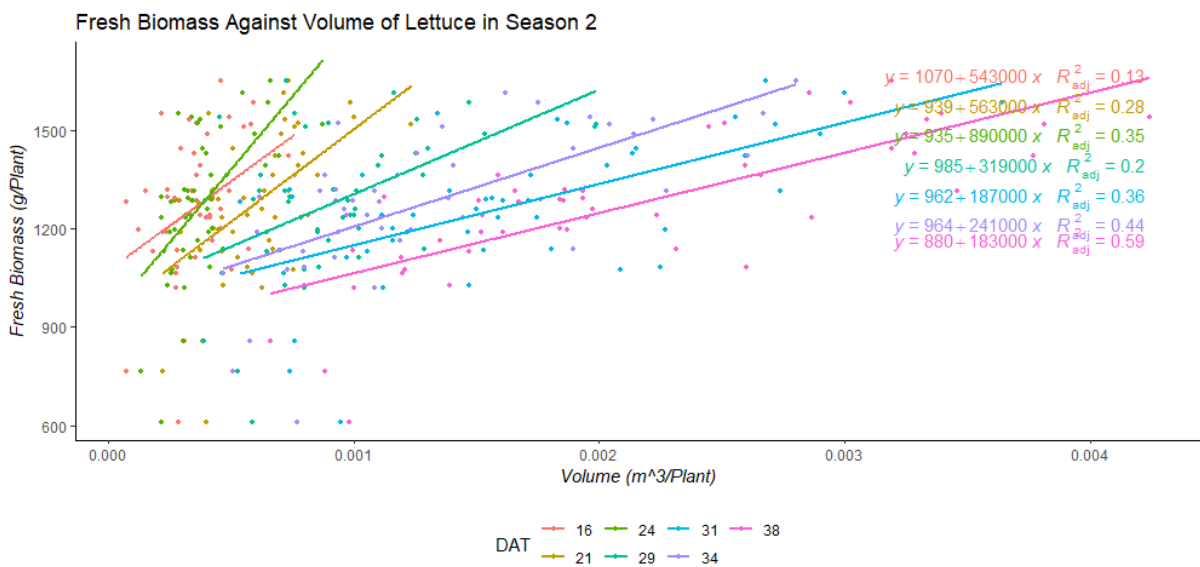


Figure 4-17 The correlations between fresh biomass and plant biovolume of final harvest plots in Season 2 fitted with linear regression.

4-5. Marketable Harvest Index (MHI)

Figure 4-18 showed the distribution of biomass after market-standard trimming process ranked from the smallest to the largest. From Figure below, the biomass from Season 2 was on average greater, but with more variability than from Season 1, and lettuce in Season 2 had higher average biomass as well as MHI values than in Season 1.

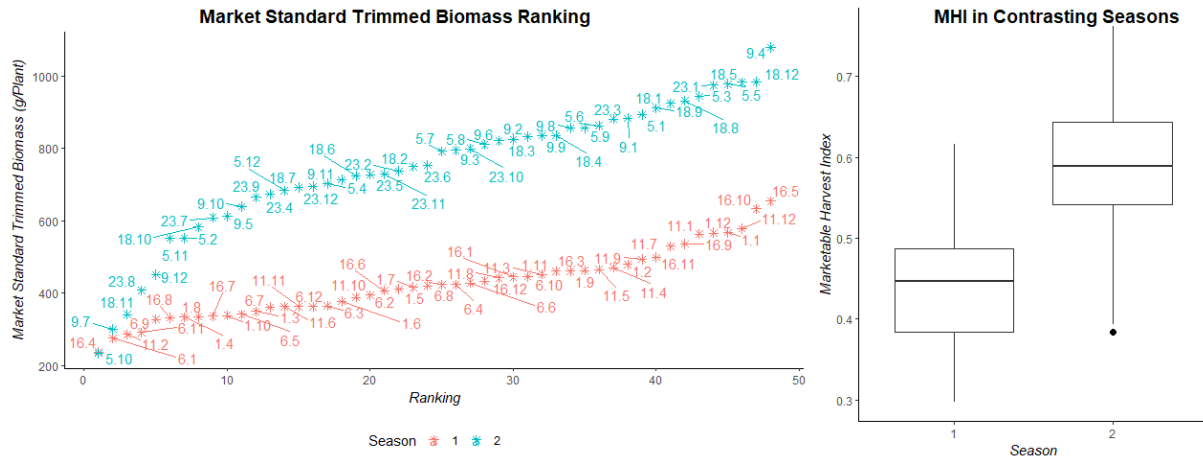





Figure 4-18 Plants from final harvest in each season were ranked based on Market Standard Trimmed Biomass (L), Labels: Plant ID. Marketable Harvest Index (MHI) in contrasting seasons (R).

In the final harvest in Season 2, the visual disease evaluation was made because Lettuce Big-Vein Virus (LBVV) was reported. The disease pressure could cause a huge reduction in biomass; thus, it could be classified into three categories based on fresh biomass: “A” (experiencing no/little disease pressure, good), “B” (experiencing medium disease pressure, marginal failure) and “C” (experiencing severe disease pressure, failure). Table 4-3 presents the three categories of lettuce and its biomass.

Table 4-3 Classifications of lettuce based on biomass.

Classification	A	B	C
Cross sections			
Weights (g)	≥ 710	450-710	≤ 451
Rankings	17 th ~48 th (~65%)	6 th ~17 th (~23%)	1 st ~5 th (10.5%)

From Table 4-3, the cross-section view of each type of lettuce made a very clear arbitration and implicit discrimination of lettuce quality. Type “A” lettuce had solid and compacted inner structure due to higher density in the core; whereas Type “B” had less dense and more hollow space than Type “A”, in contrast to other two, Type “C” presented juvenile and yellow leafy structure, and the size was the smallest of all. The results showed approximately a third of lettuces in this paddock suffer a certain degree of disease pressure.

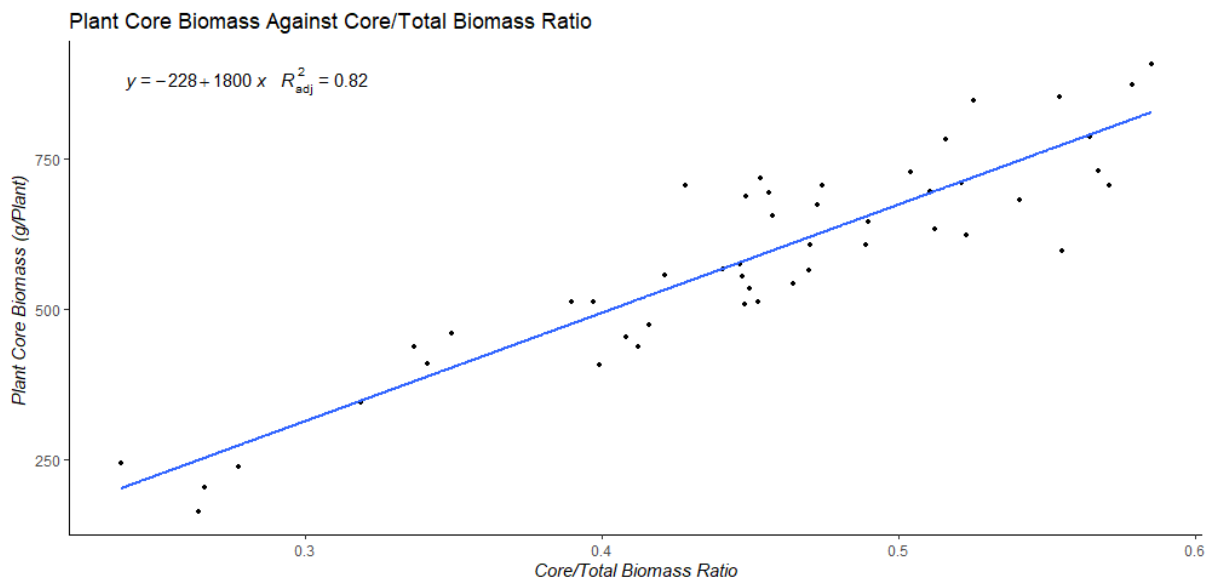


Figure 4-19 Plant Core Biomass was plotted against Core/Total Biomass Ratio for Season 2 fitted with linear regression.

Figure 4-19 suggested that there was a strong relationship (*adjusted R*² 0.82) between core biomass and core/total biomass ratio in Season 2 where the virus was found. It concluded that the core biomass of a plant was closely associated with the ratio, which means the higher core/total biomass ratio could lead to higher plant core biomass.

4-6. Light interception and Light Use Efficiency (LUE)

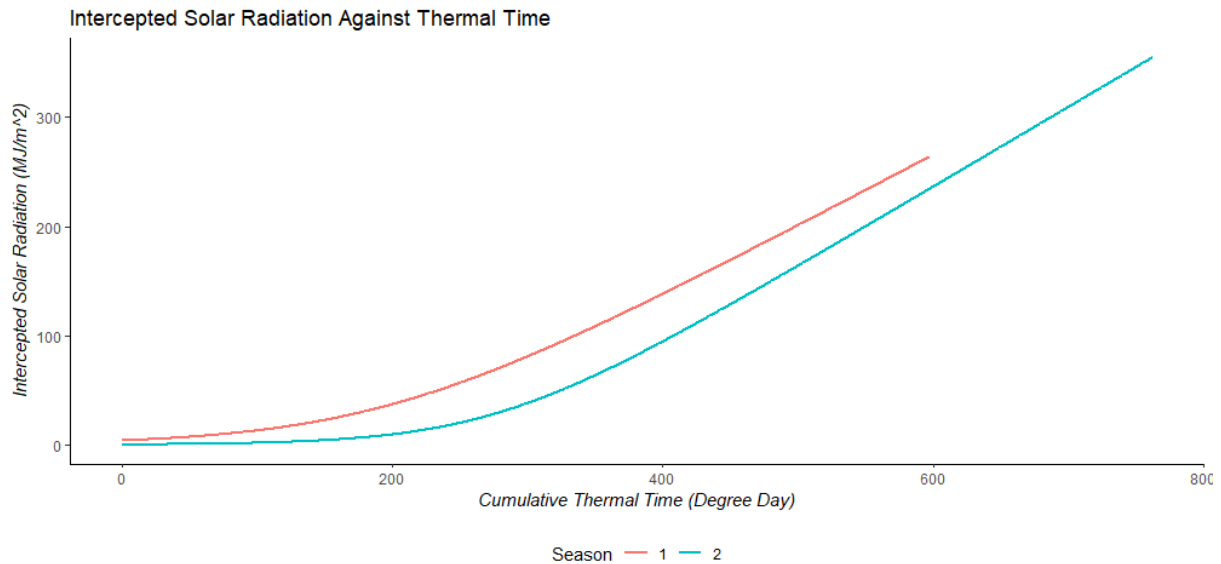


Figure 4-20 Intercepted radiation was plotted against Cumulative Thermal Time fitted with the expo-linear model from the first harvest.

Using the fit of plant leaf area against thermal time, it was possible to adjust the accumulated incident radiation (Figure 4-3) to account for the amount of light intercepted (*ie Cumulative Intercepted Solar Radiation, CumINTR*) (Figure 4-20). The model was suggested by Goudriaan and Monteith (1990) to “describe the transition from exponential to linear growth”. The expo-linear model had an equation of $CumINTR = \frac{0.6523}{0.013} \times \log_e [1 + e^{0.013 \times (TT - 19.32)}]$ in Season 1, and $CumINTR = \frac{0.73069}{0.01769} \times \log_e [1 + e^{0.01769 \times (TT - 276.68438)}]$ in Season 2.

In order to estimate the values of Light Use Efficiency for two seasons, dry matter difference for successive harvests was plotted against model-fitted intercepted solar radiation (Figure 4-20) for the harvested plants through the season in Figure 4-21; therefore, the slope is the LUE

values based on Equation 3-2. The linear regression in Figure 4-21 enabled the prediction of LUE based on average temperature. Table 4-4 exhibited lettuce at early stages has lower LUE than in all growth stages, and the lower temperature can cause decreasing LUE.

Light use efficiency was calculated from dry weight difference between two seasons had little difference and values ranged from 1.3 to 1.6 g MJ⁻¹, which is in the range of LUE typically observed for C₃ crop and plant species. The results showed that the effect of LUE was similar for both seasons, and so any effect of temperature was via impacts on the pattern of the fraction of interception of radiation. A lower temperature could extend the growth period and slow down many key plant physiological traits over the whole course of the growth period, such as dry matter weights and water content.

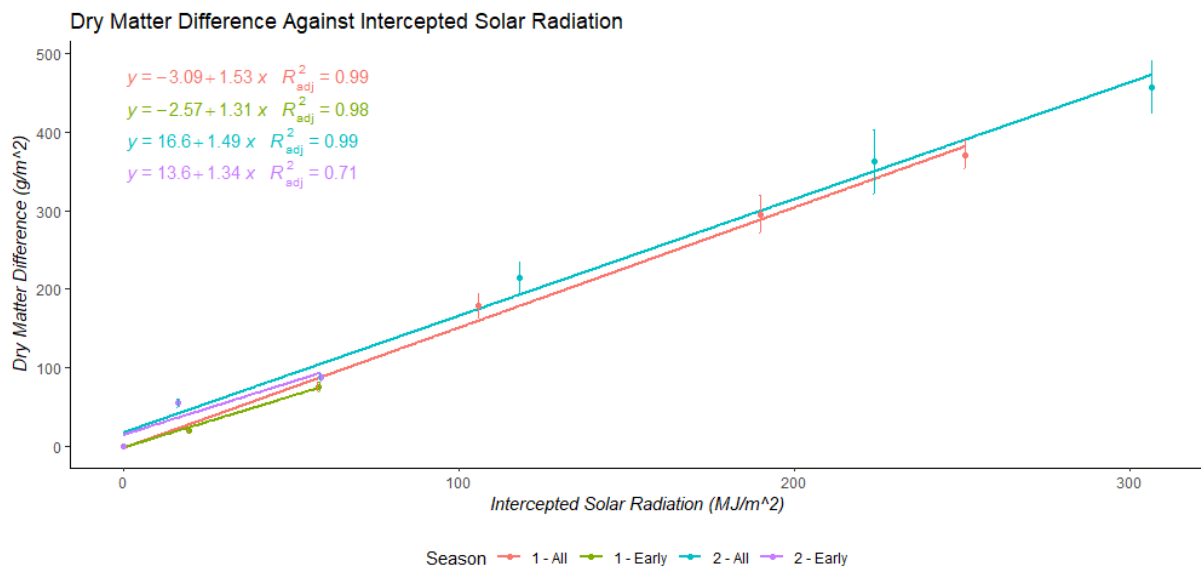


Figure 4-21 The relationships between dry matter difference and intercepted solar radiation for two seasons at early stages and whole growth stages fitted with linear regression.

Table 4-4 Summary of the relationships between Light Use Efficiency (LUE) and Average Temperature (AvgTemp) on lettuce in the early stages and the whole growth stages.

Season	LUE (g/MJ)	SE	AvgTemp (°C)
1 – Early	1.31	0.4103	17.77
2 – Early	1.34	0.3999	15.60
$LUE = 1.55567 - 0.01382 \times AvgTemp$			
1 – All	1.53	0.0776	17.12
2 – All	1.49	0.0630	14.88
$LUE = 1.22429 + 0.01786 \times AvgTemp$			

4-7. Lettuce growth simulation

Based on previous findings and results, the models from two seasons this year were applied to simulate the lettuce growth over last two decades (2000-2020) with four potential growth periods (40, 50, 60, 70 DAT) starting from 9 April and 19 May each year.

Table 4-5 Fitted curves for crop growth by fraction of intercepted radiation (*fINT*, -), Cumulative Intercepted Solar Radiation (*CumINTR*) and water content (per plant) against Cumulative Thermal Time (°Cd).

Response Variables	Explanatory Variable(s)	Models
<i>fINT</i>	Cumulative Thermal Time	$fINT = e^{0.0112329TT - 4.1815558} \quad (0 < TT < 372.26^\circ Cd)$ $fINT = 1.0 \quad (TT > 372.26^\circ Cd)$
Water Content		$\frac{0.9630}{1 + e^{\left[-\frac{1}{157.0}(TT + 231.5)\right]}}$
<i>CumINTR</i>		$\frac{0.73069}{0.01769} \times \log_e [1 + e^{0.01769 \times (TT - 276.68438)}]$

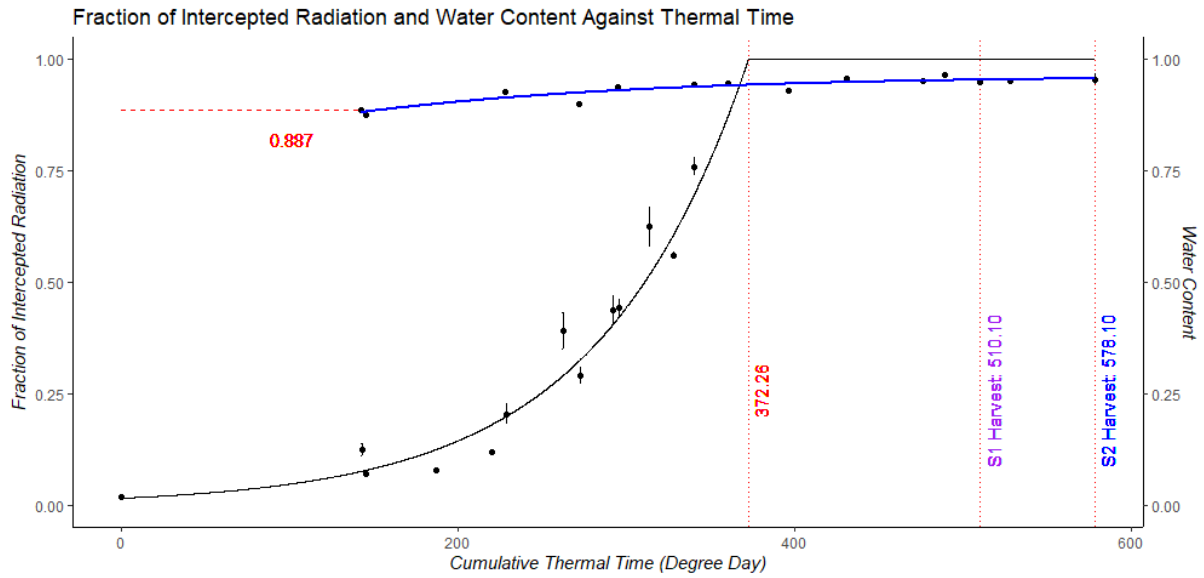


Figure 4-22 Fraction of Intercepted Radiation and Water Content ($Quasi-R^2: 0.79$) were plotted against Cumulative Thermal Time in contrasting seasons fitted with exponential curves started from the dates of transplanting when $T_b = 7^\circ C$. (maximum fraction of intercepted radiation = 1).

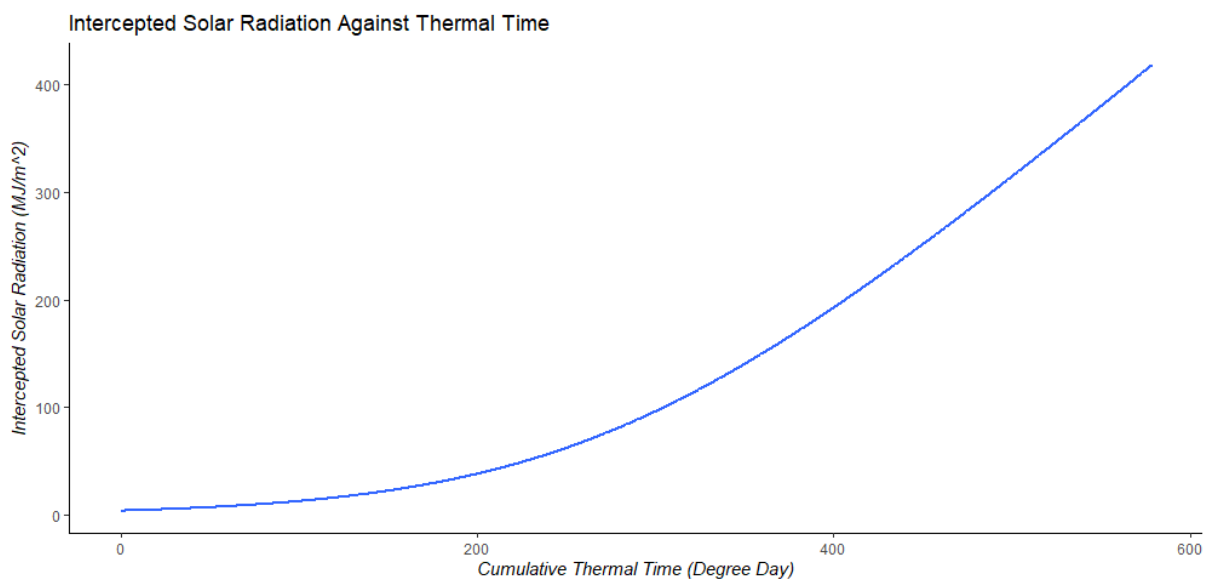


Figure 4-23 Intercepted radiation was plotted against Cumulative Thermal Time fitted with the expo-linear model when $T_b = 7^\circ C$.

Using the fINT equation above, the accumulated radiation from transplanting was re-calculated and plotted against dry and fresh weight (g/m^2) to re-estimate the LUE. The LUE for each season was similar to that already estimated (Table 4-6).

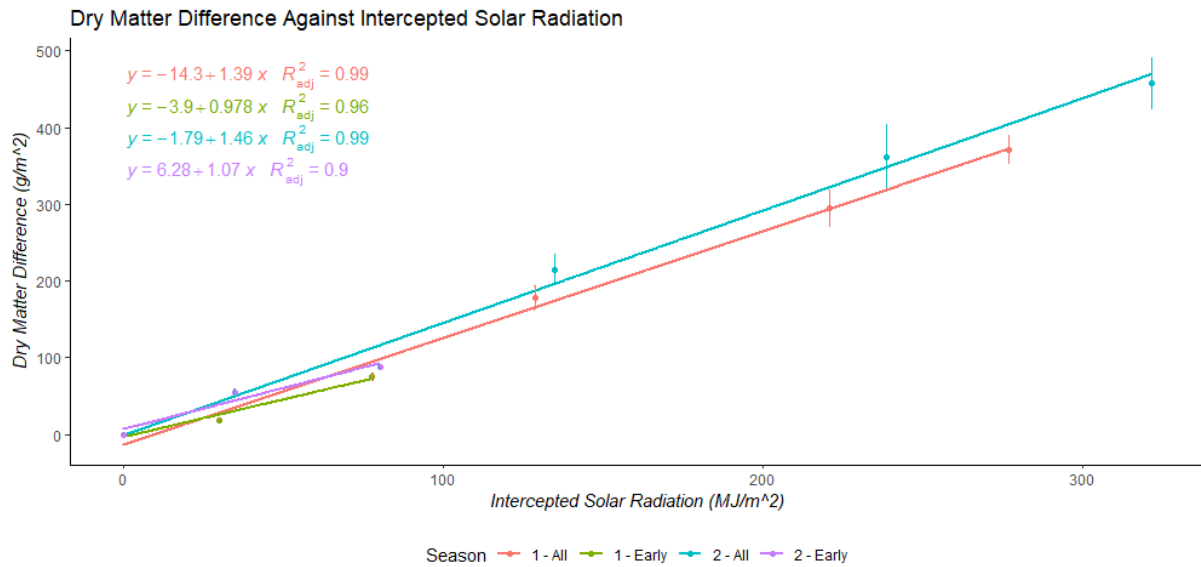


Figure 4-24 The relationships between dry matter difference and intercepted solar radiation for two seasons at early stages and whole growth stages fitted with linear regression, when $T_b = 7^\circ\text{C}$.

Table 4-6 Recalculated Light Use Efficiency when $T_b = 7^\circ\text{C}$.

Season	LUE (g/MJ)	SE	AvgTemp ($^\circ\text{C}$)
1 – Early	0.978	0.2908	17.77
2 – Early	1.07	0.2841	15.60
$LUE = 1.22257 - 0.01429 \times \text{AvgTemp}$			
1 – All	1.39	0.0665	17.12
2 – All	1.46	0.0583	14.88
$LUE = 1.92500 - 0.03125 \times \text{AvgTemp}$			

Thus, fresh biomass per plant at any thermal time can be calculated by following equation:

$$FW = \frac{DW}{(1 - WC(TT)) \times 12} = \frac{CumINTR \times LUE}{(1 - WC(TT)) \times 12} = "LUE_{FW}" \times CumINTR \div 12$$

Equation 4-1

Using the T_b of 7 °C, the TTFH for seasons 1 and 2 was 510 °Cd (48 days) and 578 °Cd (68 days), respectively. When simulated against the 20-year record, the distribution of season length (in days) for these TTFH ranged between 40 and 50 days for Season 1 (Figure 4-25) and 60 and 70 days for Season 2 (Figure 4-26).

Using the 20-year record, the fINT was computed (as shown in Figure 4-22) to calculate radiation capture over time, and the estimated LUE (Figure 4-24) was used to calculate dry biomass per square metre. Observed moisture content increased from about 85% at transplanting (estimated) to 95% from the time of full cover through to maturity (Figure 4-22). This allowed computation of fresh biomass per square metre over time. The dry and fresh biomass were estimated for each year at the TTFH. Assuming a transplanting density of 12 plants /m², the weight per plant was calculated.

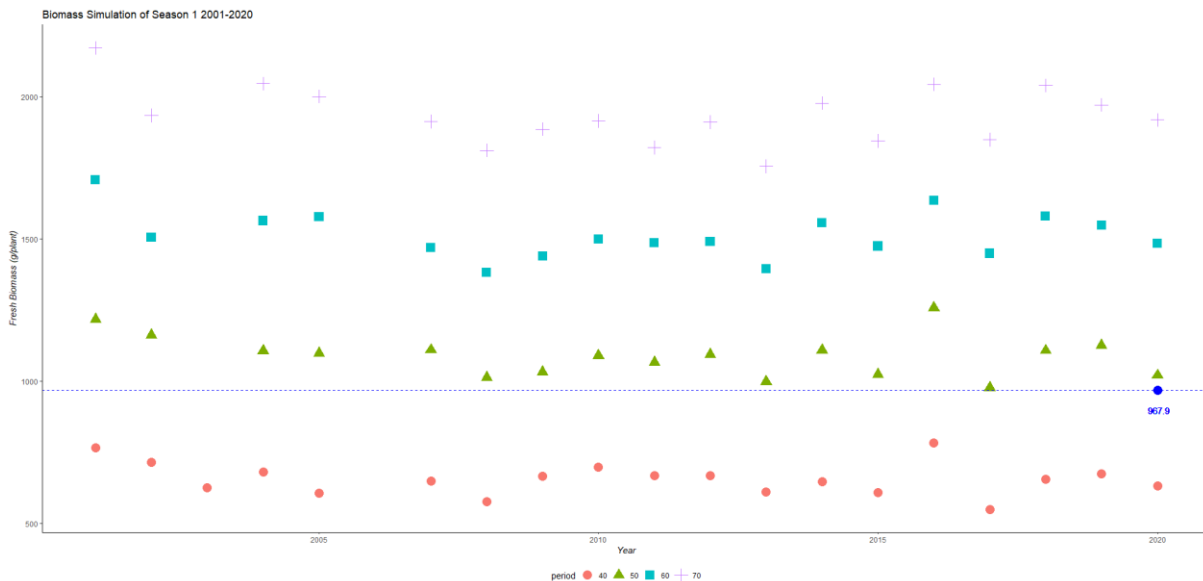


Figure 4-25 Fresh biomass was simulated from 2001 to 2020, when $T_b = 7^\circ\text{C}$ for Season 1 over different (40, 50, 60, 70 DAT) periods of growth after transplanting.

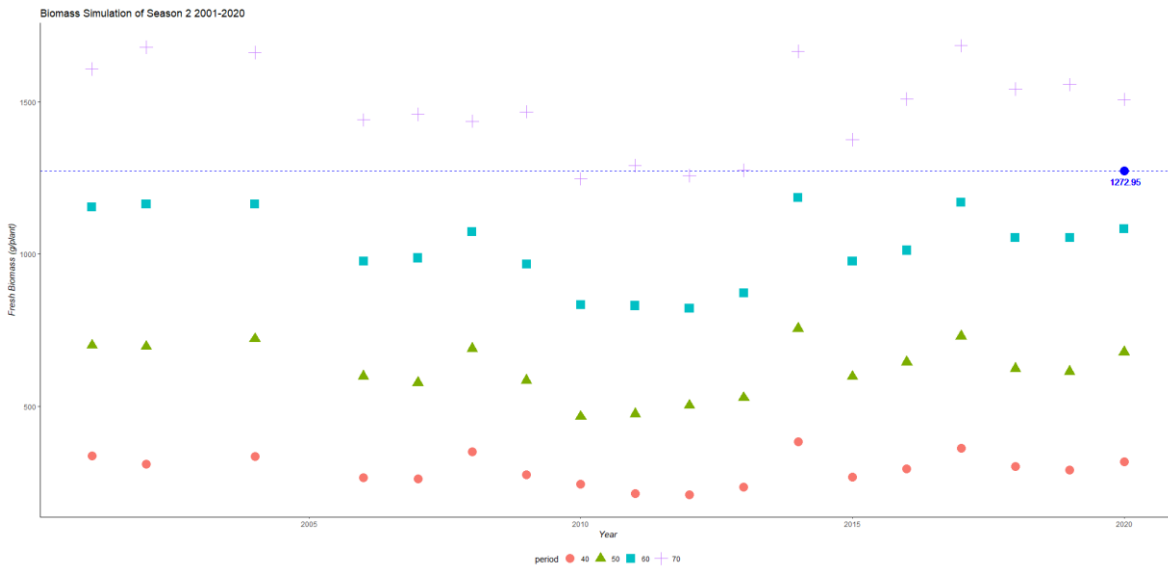


Figure 4-26 Fresh biomass was simulated from 2001 to 2020, when $T_b = 7^\circ\text{C}$ for Season 2 over different (40, 50, 60, 70 DAT) periods of growth after transplanting.

The results for 9 April and 19 May transplanting show how much the average plant weight would vary with harvest calendar date over a 20-year period (Figure 4-27). For a given calendar time to harvest, it seems that the final biomass has increased over time. This is associated with warmer temperatures, and faster development of the plants so that they intercept more radiation for a given time period. In 2020, the estimation is that plants will reach the same harvest weight about 2-5 days earlier than 2000.

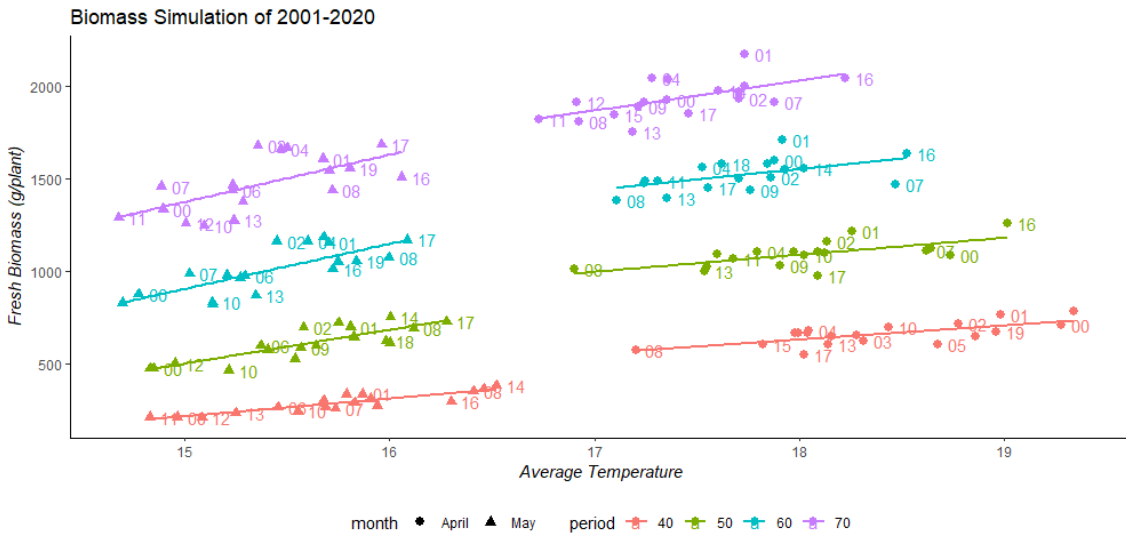


Figure 4-27 Fresh Biomass was simulated against average temperature over a 20-year period. Labels: 20yy format of years.

5. DISCUSSION

5-1. Growing conditions

Over two growing seasons, lettuce crops experienced a continuation of colder weather and shorter photoperiod. In the cooler season, the lettuce grew slower and for a longer period and intercepted more radiation from the day of transplanting. Figure 4-3 and Figure 4-20 show total radiation intercepted from the first harvest in Season 1 = 263.6 MJ/m²; Season 2 = 354.8 MJ/m². The lettuces in both seasons received the same amount of cumulative incident solar radiation and required similar intercepted solar radiation, yet the growth rate during the colder season was slower. There was a total of rainfall of 10.6 mm and 51.2 mm over two growing seasons, respectively. However, the lettuce was well-irrigated and the soil that the trial was conducted and has a higher water holding capacity with heavy clay A/C profiles (Virmani *et al.* 1982). Therefore, water stress is unlikely to have happened in the field.

5-2. Biomass accumulation and growth rates

The growth rates of lettuce are closely linked to the fraction of intercepted solar radiation and temperature as the light use efficiency is not significantly different between two seasons. Figure 5-1 uncovered the modelled cumulative intercepted could relatively predict the real-time fresh biomass and conformed that this behavioural trend could apply to both of season as two linear curves have almost identical slopes (S1:35.8; S2:34.7). Combined with previous results, it is concluded that the fresh biomass in real-time can be directly predicted at early stages.

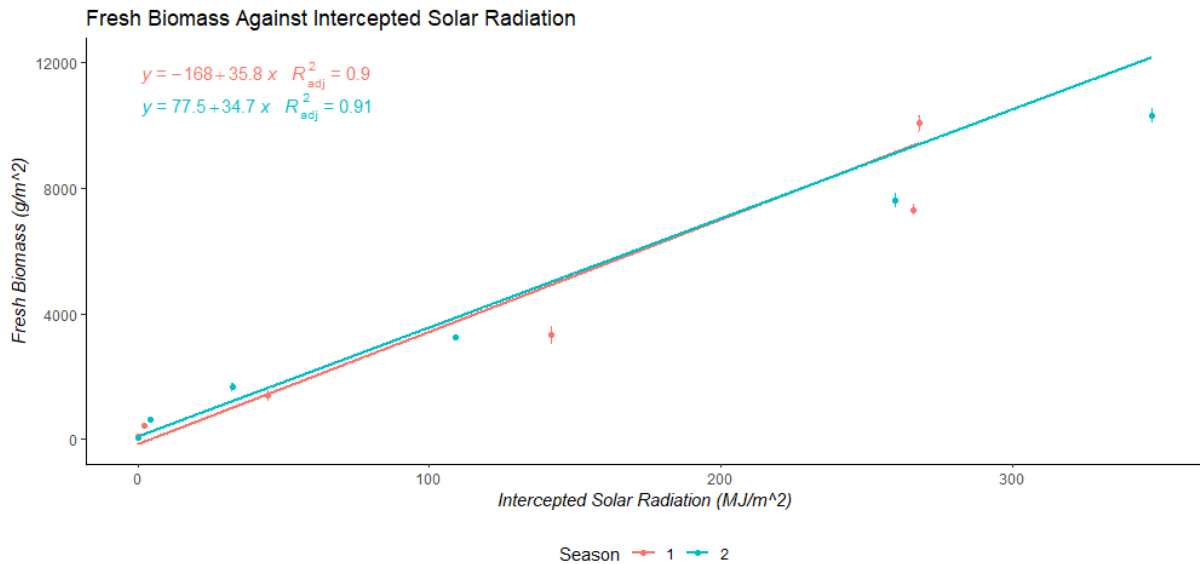


Figure 5-1 The correlations between fresh biomass and cumulative intercepted solar radiation fitted with linear regression.

5-3. Lettuce growth simulation

In this report, we have used a base temperature of 0°C, which was proposed in the literature (Wurr & Fellows 1984; Wheeler *et al.* 1993a; Wheeler *et al.* 1993b). In an irrigated crop under good nutrition, leaf area is largely dependent on temperature, so for a given planting density, it might be expected that the pattern of fINT should be effectively the same across different seasonal temperatures. A “correct” base temperature would bring all of the fINT together from multiple experiments in the same conditions (*eg* irrigated, commercial field farm) so that they overlap. Using $T_b = 0^\circ\text{C}$, the two curves from Figure 4-5 did not overlap, so these were recomputed assuming different base temperatures between 0 and 10°C. Assuming base temperature is 7 °C as shown in Figure 4-22, which is the best fit amongst all potential base temperatures from 0 °C to 10 °C (data not shown), the model of fINT against cumulative thermal time fitted both seasons. In this figure, it is apparent that in Season 2, the crop was allowed to grow for a longer period (in calendar day and thermal time), intercepting radiation at $\text{fINT} \approx 1.0$ for a longer time. To verify this estimate of a different base temperature, more data are needed.

5-4. Lettuce simulation and effects of seeding size and transplant shock

The results presented above have been based on ‘average’ plants. However, a farmer is also interested in predicting the potential variation in final plant weight. For example, at 3 weeks after transplanting, there were some variations in plant size due to both variations in seedling size and in ‘transplant shock’ (Figure 5-2). According to the Figure 4-22 and Table 4-5 when $T_b = 7^\circ\text{C}$, the fINT (fINT_n) of an average plant would be 0.253 at 21 DAT, *ie* the plant would be covering about ¼ of the final space that it can occupy when it completely covers the soil.

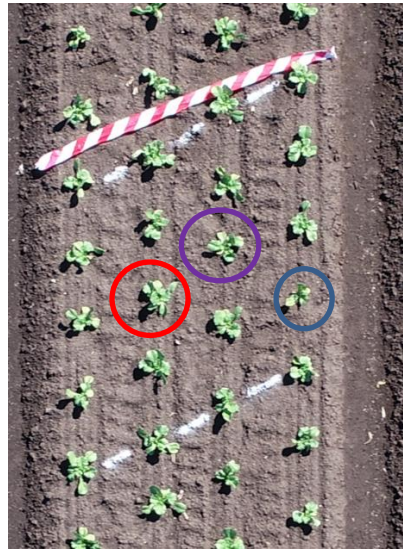


Figure 5-2 Aerial view of lettuce plants after three weeks after transplanting. Circled: blue- smaller than average size, purple- average size, red- larger than average size.

We considered the situation at 21 DAT where a plant was either half (fINT_{1/2} = 0.1265) or 50% larger than the size of the average plant (fINT_{1.5} = 0.38) at 21 DAT. These plants can be considered, respectively, as either being ‘slow’ or ‘fast’ in their development, compared to the average plant. To compute their ‘effective’ size at any time, we need to push them forward or backward along the curve of TT vs fINT, but they would still be harvested at the same thermal time or calendar time as the average plant.

$$TT = \frac{\ln(fINT) + 4.1815558}{0.0112329}$$

Equation 5-1

On the standard curve of TT vs fINT, the cumulative thermal time for fINT_{1/2} is 188.2 °Cd, for fINT_{1.5} is 286.1°Cd and for fINT_n is 250 °Cd. If we consider the 2020 Season 1 experiment, final harvest was at 510 °Cd when DAT = 48. Figure 5-3 shows the pattern of fINT that would occur in the time from transplant to harvest (27 days). For this period the accumulated radiation interception would be CumINTR_{1/2} = 183.8 MJ/m², CumINTR_{1.5} = 316.7 MJ/m², CumINTR_n = 274.4 MJ/m². Using the estimated LUE from the two seasons, we then estimate the final fresh weight at the final harvest by using Equation 4-1: FW_{1/2} = 479.8 g, FW_{1.5} = 825.7 g, FW_n = 716.1 g per plant at the harvest day.

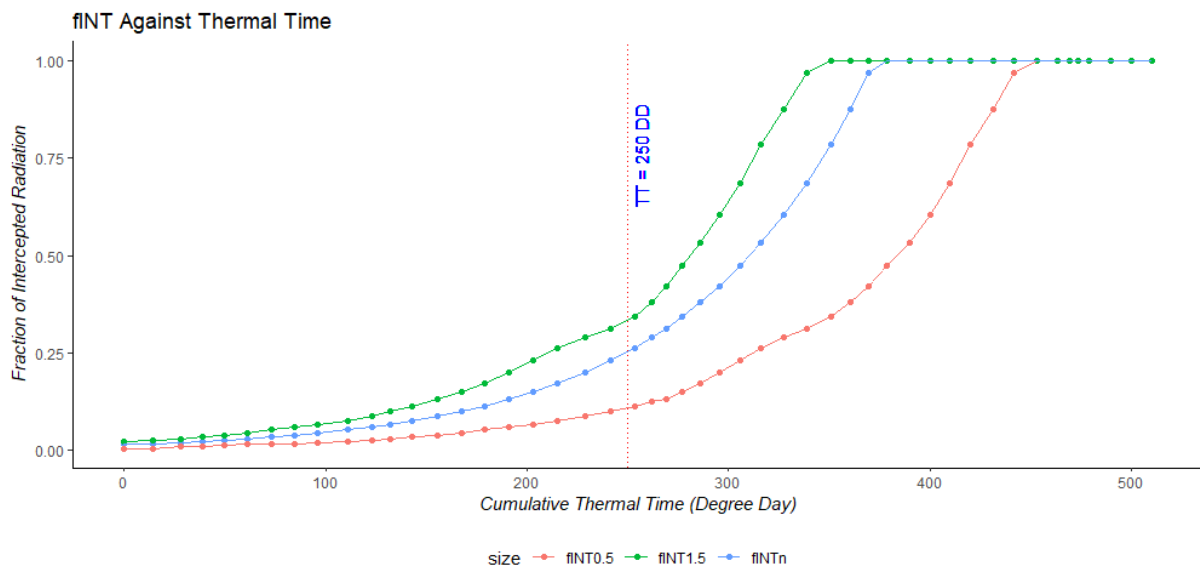


Figure 5-3 Trends of fINT against Cumulative Thermal Time of three sizes of lettuce (fINT: 50% smaller, Average size, 50% larger)

5-5. Crop modelling on lettuce

Plant dry matter has been considered as a key to building the relationship between crop production and the environment. Fresh weight, is not always consistent with dry weight in horticultural crops, but the dry matter is still important estimation of yield, which was predominately determined by water content (Both *et al.* 1997; Marcelis *et al.* 1998). Previous studies about lettuce modelling have been concentrating in the greenhouse environment, for example, Lin (2002) used Artificial neural networks (ANN) to model the final fresh weight according to the weekly average of daily light, and van Henten (1994) suggested that the leaf

area could be simulated by leaf dry weight for lettuce with a hyperbolic model (Marcelis *et al.* 1998). However, no literature has been found that image analysis from UAV images has been used to measure plant area in order to predict lettuce biomass in the natural environment.

5-6. Remote sensing applications

Many methods in remote sensing have been employed to assess the horticultural crops (Davenport *et al.* 2005; Campillo *et al.* 2008). Different studies have applied remote sensing to assess biophysical characters of certain types of crops, such as potato, wheat, poppy, maize, rice, sunflower, corn and barley (Iqbal *et al.* 2017). Bumgarner *et al.* (2012) applied overhead images taken from commercial digital cameras to estimate lettuce area and biomass in the outdoor, high tunnel, and greenhouse settings showing all correlations are significant and positive. Ren *et al.* (2017) and Osco *et al.* (2019) used multi- or hyper-spectral to evaluate lettuce health and water stress. Furthermore, Jung *et al.* (2015) developed the two image-processing methods (morphological and colour-value analysis) to estimate fresh biomass of lettuce in a hydroponic system.

5-7. Disease impact on lettuce biomass production

In Season 2, lettuce big-vein disease (LBVD) was observed. The disease is caused by the causal agent *lettuce big-vein associated virus* (LBVaV, genus *Varicosavirus*) (Verbeek *et al.* 2013). It is responsible for showing the characteristics of necrotic “big-vein” symptoms of breeding lines - enlargements and thickening veins potentially with severe deformation of leaves, vein clearing, leaf crinkling, and susceptible to be tested by viruliferous *Olpidium virulentus* spores in a nutrient film technique (NFT) system (Verbeek *et al.* 2013; Umar *et al.* 2017). The lettuce biomass reduction caused by LBVD shows unsightly vegetation, in terms of creating late head formation, shrinking of the head, and lower harvestable percentage (Umar *et al.* 2017).

5-8. Marketable Harvest Index (MHI)

The marketable part of lettuce is its core part in the head, which decides the quality and weight of each lettuce. The formation and consolidation of core part in lettuce head is happening in later stages of growth, which means early harvest (*ie* Season 1) can cause lower core weights, in return lower MHI values. The MHI helps to understand how much that marketable value in

each lettuce head. In general, the heavier lettuce is, the higher proportion of core weight is (Figure 4-18). This is because premium-level lettuce has very dense and solid core part as shown as Type “A” lettuce in Table 4-3.

5-9. Future research directions

Due to time limitations for experimentation, there is still scope to improve these models in future research. In this project, only four blocks of lettuce were surveyed and harvested over the autumn/winter season located in two paddocks, meaning that the experiments lacked replications across multiple environments. In further studies, it would be better to set more replications and harvests over different fields, sites, cultivars, time of the year as well as fly UAVs more frequently around three weeks after transplanting (400 °Cd). As for destructive sampling, it would be possible to investigate core weight development or core/total ratio over thermal time comparing against the plot of fINT over thermal time.

6. CONCLUSION

Biomass is a crucial measure of crop development and production, and remote sensing has a high potential to assess actual crop condition and growth through high-definition images (Hunt *et al.* 2005). In this experiment, biomass can be estimated from plant dimensions, however, accuracy was not as good as expected, and the final biomass could be predicted through the model at 400 °Cd (3 weeks after transplanting). Colder temperatures in winter could help expand surveys in order to improve model accuracy, as temperature and intercepted solar radiation are the key factors to lettuce growth rate rather than light use efficiency indicated by a marginal difference in light use efficiency. Plant disease, particularly Lettuce Big-Vein Virus, was a constraint for lettuce biomass production in Season 2.

7. REFERENCES

ABCB 2015, *Climate zone map: Australia wide*, Australian Building Codes Board, viewed 21 May 2020, <<https://www.abcb.gov.au/Resources/Tools-Calculators/Climate-Zone-Map-Australia-Wide>>.

Anten, NPR 2004, 'Optimal photosynthetic characteristics of individual plants in vegetation stands and implications for species coexistence', *Annals of Botany*, vol. 95, no. 3, pp. 495-506.

ASPS 2018, *Chapter 6 - Growth analysis: a quantitative approach*, Australian Society of Plant Scientists, Brisbane, Queensland
<<http://plantsinaction.science.uq.edu.au/content/chapter-6-growth-analysis-quantitative-approach>>.

Ballesteros, R, Ortega, JF, Hernandez, D & Moreno, MA 2018, 'Onion biomass monitoring using UAV-based RGB imaging', *Precision Agriculture*, vol. 19, no. 5, pp. 840-57.

Bendig, J, Bolten, A, Bennertz, S, Broscheit, J, Eichfuss, S & Bareth, G 2014, 'Estimating Biomass of Barley Using Crop Surface Models (CSMs) Derived from UAV-Based RGB Imaging', *Remote Sensing*, vol. 6, no. 11, pp. 10395-412.

Bendig, J, Yu, K, Aasen, H, Bolten, A, Bennertz, S, Broscheit, J, Gnyp, ML & Bareth, G 2015, 'Combining UAV-based plant height from crop surface models, visible, and near infrared vegetation indices for biomass monitoring in barley', *International Journal of Applied Earth Observation and Geoinformation*, vol. 39, pp. 79-87.

Bensink, J 1971, 'On morphogenesis of lettuce leaves in relation to light and temperature', Wageningen University

Betts, RA 2005, 'Integrated approaches to climate–crop modelling: needs and challenges', *Philosophical Transactions of the Royal Society B: Biological Sciences*, vol. 360, no. 1463, pp. 2049-65.

Bisbis, MB, Gruda, N & Blanke, M 2018, 'Potential impacts of climate change on vegetable production and product quality – A review', *Journal of Cleaner Production*, vol. 170, pp. 1602-20.

Blum, A 2011, *Plant Breeding for Water-Limited Environments*, 1st edn, Springer New York, New York, NY.

BOM 2001, *Map of Climate Zones of Australia*, Bureau of Meteorology, viewed 21 May 2020, <<http://www.bom.gov.au/climate/how/newproducts/images/zones.shtml>>.

Both, AJ, Albright, LD, Langhans, RW, Reiser, RA & Vinzant, BG 1997, 'Hydroponic lettuce production influenced by integrated supplemental light levels in a controlled environment agriculture facility: Experimental results', in T Blacqui re (ed.), *III International Symposium on Artificial Lighting in Horticulture*, Noordwijkerhout, Netherlands pp. 45-52.

Bouman, B 1995, 'Crop modelling and remote sensing for yield prediction', *NJAS wageningen journal of life sciences*, vol. 43, no. 2, pp. 143-61.

Breiman, L, Friedman, J, Olshen, R & Stone, C 1984, *Classification and Regression Trees*, Wadsworth International Group, Belmont, California, USA.

Buitenwerf, R, Rose, L & Higgins, SI 2015, 'Three decades of multi-dimensional change in global leaf phenology', *Nature Climate Change*, vol. 5, no. 4, pp. 364-8.

Bumgarner, NR, Miller, WS & Kleinhenz, MD 2012, 'Digital Image Analysis to Supplement Direct Measures of Lettuce Biomass', *HortTechnology hortte*, vol. 22, no. 4, p. 547.

Bureau of Meteorology 2020, *Climate statistics for Australian locations: Gatton DAFF Research Station*, viewed 30 August 2020, <http://www.bom.gov.au/climate/averages/tables/cw_040082.shtml>.

Calvin, M & Bassham, JA 1962, *The photosynthesis of carbon compounds*, W.A. Benjamin, New York, N.Y.

Campbell, GS 1986, 'Extinction coefficients for radiation in plant canopies calculated using an ellipsoidal inclination angle distribution', *Agricultural and Forest Meteorology*, vol. 36, no. 4, pp. 317-21.

Campillo, C, Prieto, MH, Daza, C, Mo nino, MJ & Garc a, MI 2008, 'Using Digital Images to Characterize Canopy Coverage and Light Interception in a Processing Tomato Crop', *HortScience horts*, vol. 43, no. 6, p. 1780.

Carey, D, Deuter, P, Zull, A, Taylor, H & White, N 2017, *Activity 1-Assessing horticulture Crops Suitability for the Queensland Murray Darling Basin Study Area*, Queensland Government Department of Agriculture and Fisheries, Brisbane, Queensland.

Davenport, JR, Stevens, RG, Perry, EM & Lang, NS 2005, 'Leaf Spectral Reflectance for Nondestructive Measurement of Plant Nutrient Status', *HortTechnology horttech*, vol. 15, no. 1, p. 31.

de Wit, CT 1958, *Transpiration and crop yields*, vol. 64, Versl Landabouwk Onderz Wageningen, Netherland.

De Wit, CT 1969, 'Dynamic concepts in biology', in *Prediction and measurement of photosynthetic productivity. Proceedings of the IBP/PP Technical Meeting, Trebon, 1969*, pp. 17-23.

Deuter, P, White, N & Putland, D 2012, *Critical temperature thresholds-case study lettuce* Managing Climate Variability R&D Program, Brisbane, Queensland.

DJI n.d., *Phantom 4 Advanced Specs*, viewed September 24 2020, <<https://www.dji.com/au/phantom-4-adv/info>>.

Drew, RLK & Brocklehurst, PA 1990, 'Effects of Temperature of Mother-plant Environment on Yield and Germination of Seeds of Lettuce (*Lactuca sativa*)', *Annals of Botany*, vol. 66, no. 1, pp. 63-71.

Duan, T, Zheng, B, Guo, W, Ninomiya, S, Guo, Y & Chapman, SC 2017, 'Comparison of ground cover estimates from experiment plots in cotton, sorghum and sugarcane based on images and ortho-mosaics captured by UAV', *Functional Plant Biology*, vol. 44, no. 1, pp. 169-83.

Evans, JP, Meng, X & McCabe, MF 2017, 'Land surface albedo and vegetation feedbacks enhanced the millennium drought in south-east Australia', *Hydrology and Earth System Sciences*, vol. 21, no. 1, pp. 409-22.

Evans, LT 1993, *Crop evolution, adaptation, and yield*, Cambridge University Press, Cambridge.

Felipe-García, B, Hernández-López, D & Lerma, JL 2012, 'Analysis of the ground sample distance on large photogrammetric surveys', *Applied Geomatics*, vol. 4, no. 4, pp. 231-44.

Friend, AD 2010, 'Terrestrial plant production and climate change', *Journal of Experimental Botany*, vol. 61, no. 5, pp. 1293-309.

Fu, W, Li, P & Wu, Y 2012, 'Effects of different light intensities on chlorophyll fluorescence characteristics and yield in lettuce', *Scientia Horticulturae*, vol. 135, pp. 45-51.

Gallagher, JN 1979, 'Field studies of cereal leaf growth: I. Initiation and expansion in relation to temperature and ontogeny', *Journal of Experimental Botany*, vol. 30, no. 117, pp. 625-36.

Gansert, D & Sprick, W 1998, 'Storage and mobilization of nonstructural carbohydrates and biomass development of beech seedlings (*Fagus sylvatica* L.) under different light regimes', *Trees*, vol. 12, no. 5, pp. 247-57.

Gary, C, Jones, JW & Tchamitchian, M 1998, 'Crop modelling in horticulture: state of the art', *Scientia Horticulturae*, vol. 74, no. 1, pp. 3-20.

Gauthier, NW, Kaiser, C & Klahr, M 2014, *Transplant Shock: Disease or Cultural Problem?*, University of Kentucky College of Agriculture, Food and Environment, Lexington, KY, United States.

Gil, M, Tudela, J, Martínez-Sánchez, A & Luna, M 2012, 'Harvest maturity indicators of leafy vegetables', *Stewart Postharvest Review*, vol. 8, no. 1, pp. 1-9.

Gilna, P, Lynd, LR, Mohnen, D, Davis, MF & Davison, BH 2017, 'Progress in understanding and overcoming biomass recalcitrance: a BioEnergy Science Center (BESC) perspective', *Biotechnology for Biofuels*, vol. 10, no. 1, p. 285.

González-Quiñones, JJ, Reinoso-Gordo, JF, León-Robles, CA, García-Balboa, JL & Ariza-López, FJ 2018, 'Variables Influencing the Accuracy of 3D Modeling of Existing Roads Using Consumer Cameras in Aerial Photogrammetry', *Sensors (Basel, Switzerland)*, vol. 18, no. 11, p. 3880.

Goudriaan, J & Monteith, J 1990, 'A mathematical function for crop growth based on light interception and leaf area expansion', *Annals of Botany*, vol. 66, no. 6, pp. 695-701.

Gray, D & Morris, GEL 1978, 'Seasonal effects on the growth and time to maturity of lettuce', *The Journal of Agricultural Science*, vol. 91, no. 3, pp. 523-9.

Guo, W, Rage, UK & Ninomiya, S 2013, 'Illumination invariant segmentation of vegetation for time series wheat images based on decision tree model', *Computers and Electronics in Agriculture*, vol. 96, pp. 58-66.

Gupta, S, Gowri, BS, Lakshmi, AJ & Prakash, J 2013, 'Retention of nutrients in green leafy vegetables on dehydration', *Journal of Food Science and Technology*, vol. 50, no. 5, pp. 918-25.

Hammer, GL, Kropff, MJ, Sinclair, TR & Porter, JR 2002, 'Future contributions of crop modelling—from heuristics and supporting decision making to understanding genetic regulation and aiding crop improvement', *European Journal of Agronomy*, vol. 18, no. 1, pp. 15-31.

Haxeltine, A & Prentice, IC 1996, 'A General Model for the Light-Use Efficiency of Primary Production', *Functional Ecology*, vol. 10, no. 5, pp. 551-61.

Hay, RKM 1995, 'Harvest index: a review of its use in plant breeding and crop physiology', *Annals of Applied Biology*, vol. 126, no. 1, pp. 197-216.

Hort Innovation 2019, *Australian Horticulture Statistics Handbook 2018-19: Vegetables*, Horticulture Innovation Australia, Sydney, NSW.

Hunt, ER, Cavigelli, M, Daughtry, CST, McMurtrey, JE & Walthall, CL 2005, 'Evaluation of Digital Photography from Model Aircraft for Remote Sensing of Crop Biomass and Nitrogen Status', *Precision Agriculture*, vol. 6, no. 4, pp. 359-78.

Iqbal, F, Lucieer, A, Barry, K & Wells, R 2017, 'Poppy crop height and capsule volume estimation from a single UAS flight', *Remote Sensing*, vol. 9, no. 7, p. 647.

Isbell, R 2016, *The Australian soil classification*, CSIRO publishing, Melbourne, Victoria.

James, C 2020, 'Counting and measuring lettuces via semantic image segmentation', Master of Data Science thesis, The University of Queensland.

Jenni, S & Bourgeois, G 2008, 'Quantifying Phenology and Maturity in Crisphead Lettuce', *HortTechnology hortte*, vol. 18, no. 4, p. 553.

Jung, D-H, Park, SH, Han, H & Kim, H-J 2015, 'Image processing methods for measurement of lettuce fresh weight', *Journal of Biosystems Engineering*, vol. 40, no. 1, pp. 89-93.

Kikuzawa, K 1995, 'Leaf phenology as an optimal strategy for carbon gain in plants', *Canadian Journal of Botany*, vol. 73, no. 2, pp. 158-63.

Kirkham, MB 2005, '8 - Field Capacity, Wilting Point, Available Water, and the Non-Limiting Water Range', in MB Kirkham (ed.), *Principles of Soil and Plant Water Relations*, Academic Press, Burlington, pp. 101-15.

Korres, NE, Norsworthy, JK, Tehranchian, P, Gitsopoulos, TK, Loka, DA, Oosterhuis, DM, Gealy, DR, Moss, SR, Burgos, NR, Miller, MR & Palhano, M 2016, 'Cultivars to face climate change effects on crops and weeds: a review', *Agronomy for Sustainable Development*, vol. 36, no. 1, p. 12.

Kramer, PJ 1963, 'Water Stress and Plant Growth', paper presented to Responses of Field Crops to Environmental Factors, St. Louis, Missouri.

Kristensen, S, Friis, E, Henriksen, K & Mikkelsen, SA 1987, 'Application of temperature sums in the timing of production of crisp lettuce', in DJ Cantliffe & HH Bryan (eds), *Symposium on the Timing of Field Production of Vegetables*, Tampa, Florida, USA pp. 217-26.

Lin, WC 2002, 'Crop Modelling and Yield Prediction for Greenhouse-Grown Lettuce', in JH Lieth & LR Oki (eds), *IV International Symposium on Models for Plant Growth and Control in Greenhouses: Modeling for the 21st Century - Agronomic and Greenhouse Crop Models*, Beltsville, MD, USA pp. 159-64.

- Liu, X, Deng, Z & Yang, Y 2019, 'Recent progress in semantic image segmentation', *Artificial Intelligence Review*, vol. 52, no. 2, pp. 1089-106.
- Lobell, DB & Burke, MB 2010, 'On the use of statistical models to predict crop yield responses to climate change', *Agricultural and Forest Meteorology*, vol. 150, no. 11, pp. 1443-52.
- Lorenz, HP & Wiebe, HJ 1980, 'Effect of temperature on photosynthesis of lettuce adapted to different light and temperature conditions', *Scientia Horticulturae*, vol. 13, no. 2, pp. 115-23.
- Marcelis, LFM, Heuvelink, E & Goudriaan, J 1998, 'Modelling biomass production and yield of horticultural crops: a review', *Scientia Horticulturae*, vol. 74, no. 1, pp. 83-111.
- Masson, J, Tremblay, N & Gosselin, A 1991, 'Nitrogen Fertilization and HPS Supplementary Lighting Influence Vegetable Transplant Production. I. Transplant Growth', *Journal of the American Society for Horticultural Science*, vol. 116, no. 4, p. 594.
- McMaster, GS & Wilhelm, W 1997, 'Growing degree-days: one equation, two interpretations', *Agricultural and Forest Meteorology*, vol. 87, pp. 291-300.
- Medlyn, BE 1998, 'Physiological basis of the light use efficiency model', *Tree Physiology*, vol. 18, no. 3, pp. 167-76.
- Monteith, JL 1972, 'Solar Radiation and Productivity in Tropical Ecosystems', *Journal of Applied Ecology*, vol. 9, no. 3, pp. 747-66.
- Monteith, JL 1977, 'Climate and the efficiency of crop production in Britain', *Philosophical Transactions of the Royal Society of London. B, Biological Sciences*, vol. 281, no. 980, pp. 277-94.
- Nex, F & Remondino, F 2014, 'UAV for 3D mapping applications: a review', *Applied Geomatics*, vol. 6, no. 1, pp. 1-15.
- Nicola, S & Cantliffe, DJ 1996, 'Increasing Cell Size and Reducing Medium Compression Enhance Lettuce Transplant Quality and Field Production', *HortScience* vol. 31, no. 2, p. 184.
- Noureldin, NA, Aboelghar, MA, Saady, HS & Ali, AM 2013, 'Rice yield forecasting models using satellite imagery in Egypt', *The Egyptian Journal of Remote Sensing and Space Science*, vol. 16, no. 1, pp. 125-31.
- Öquist, G 1983, 'Effects of low temperature on photosynthesis', *Plant, Cell & Environment*, vol. 6, no. 4, pp. 281-300.

Osco, LP, Ramos, APM, Moriya, ÉAS, Bavaresco, LG, Lima, BCd, Estrabis, N, Pereira, DR, Creste, JE, Júnior, JM & Gonçalves, WN 2019, 'Modeling hyperspectral response of water-stress induced lettuce plants using artificial neural networks', *Remote Sensing*, vol. 11, no. 23, p. 2797.

Peet, MM & Wolfe, DW 2000, 'Chapter 10: Crop ecosystem responses to climatic change: vegetable crops ', in KR Reddy & H Hodges (eds), *Climate change and global crop productivity*, CABI, New York, NY, USA, p. 215.

Propeller Aero 2018, *What is ground sample distance (GSD) and how does it affect your drone data?*, viewed September 24 2020, <<https://www.propelleraero.com/blog/ground-sample-distance-gsd-calculate-drone-data/?pdf=2291>>.

Qin, K & Leskovar, DI 2020, 'Humic Substances Improve Vegetable Seedling Quality and Post-Transplant Yield Performance under Stress Conditions', *Agriculture*, vol. 10, no. 7, p. 254.

Qin, L, He, J & Lee, SK 2002, 'Response of lettuce (*Lactuca sativa* L.) growth to reciprocal root-zone temperature (RZT) transfer at different growth stages', *The Journal of Horticultural Science and Biotechnology*, vol. 77, no. 6, pp. 683-90.

Raid, RN 2004, 'Lettuce Diseases and their Management', in SAMH Naqvi (ed.), *Diseases of Fruits and Vegetables: Volume II: Diagnosis and Management*, Springer Netherlands, Dordrecht, pp. 121-47.

Raju, PDR & Neelima, G 2012, 'Image segmentation by using histogram thresholding', *International Journal of Computer Science Engineering and Technology*, vol. 2, no. 1, pp. 776-9.

Ren, DD, Tripathi, S & Li, LK 2017, 'Low-cost multispectral imaging for remote sensing of lettuce health', *Journal of Applied Remote Sensing*, vol. 11, no. 1, p. 016006.

Ritchie, JT 1972, 'Model for predicting evaporation from a row crop with incomplete cover', *Water Resources Research*, vol. 8, no. 5, pp. 1204-13.

Sadok, W, Naudin, P, Boussuge, B, Muller, B, Welcker, C & Tardieu, F 2007, 'Leaf growth rate per unit thermal time follows QTL-dependent daily patterns in hundreds of maize lines under naturally fluctuating conditions', *Plant, Cell & Environment*, vol. 30, no. 2, pp. 135-46.

Sage, RF & Kubien, DS 2007, 'The temperature response of C₃ and C₄ photosynthesis', *Plant, Cell & Environment*, vol. 30, no. 9, pp. 1086-106.

Sage, RF & Zhu, X-G 2011, 'Exploiting the engine of C₄ photosynthesis', *Journal of Experimental Botany*, vol. 62, no. 9, pp. 2989-3000.

Shimizu, H, Kushida, M & Fujinuma, W 2008, 'A Growth Model for Leaf Lettuce under Greenhouse Environments', *Environmental Control in Biology*, vol. 46, no. 4, pp. 211-9.

Soribe, FI & Curry, RB 1973, 'Simulation of lettuce growth in an air-supported plastic greenhouse', *Journal of Agricultural Engineering Research*, vol. 18, no. 2, pp. 133-40.

Streck, NA 2005, 'Climate change and agroecosystems: the effect of elevated atmospheric CO₂ and temperature on crop growth, development, and yield', *Ciência Rural*, vol. 35, pp. 730-40.

Stubbs, L & Grogan, R 1963, 'Necrotic yellows: A newly recognized virus disease of lettuce', *Australian Journal of Agricultural Research*, vol. 14, no. 4, pp. 439-59.

Torres-Sánchez, J, López-Granados, F & Peña, JM 2015, 'An automatic object-based method for optimal thresholding in UAV images: Application for vegetation detection in herbaceous crops', *Computers and Electronics in Agriculture*, vol. 114, pp. 43-52.

Umar, M, Amer, MA, Al-Saleh, MA, Al-Shahwan, IM, Shakeel, MT, Zakri, AM & Katis, NI 2017, 'Characterization of lettuce big-vein associated virus and Mirafiori lettuce big-vein virus infecting lettuce in Saudi Arabia', *Archives of Virology*, vol. 162, no. 7, pp. 2067-72.

van Henten, EJ 1994, 'Validation of a dynamic lettuce growth model for greenhouse climate control', *Agricultural Systems*, vol. 45, no. 1, pp. 55-72.

Verbeek, M, Dullemans, AM, van Bekkum, PJ & van der Vlugt, RAA 2013, 'Evidence for Lettuce big-vein associated virus as the causal agent of a syndrome of necrotic rings and spots in lettuce', *Plant Pathology*, vol. 62, no. 2, pp. 444-51.

Virmani, S, Sahrawat, K & Burford, J 1982, 'Physical and chemical properties of Vertisols and their management', paper presented to Twelfth International Congress of Soil Science, New Delhi, India, 8-16 February 1982.

Waller, S & Lewis, J 1979, 'Occurrence of C₃ and C₄ photosynthetic pathways in North American grasses', *Rangeland Ecology & Management/Journal of Range Management Archives*, vol. 32, no. 1, pp. 12-28.

Weston, LA & Zandstra, B 1986, *Effect of root container size and location of production on growth and yield of tomato transplants*.

Wheeler, T, Hadley, P, Ellis, R & Morison, J 1993a, 'Changes in growth and radiation use by lettuce crops in relation to temperature and ontogeny', *Agricultural and Forest Meteorology*, vol. 66, no. 3-4, pp. 173-86.

Wheeler, TR, Hadley, P, Morison, JIL & Ellis, RH 1993b, 'Effects of temperature on the growth of lettuce (*Lactuca sativa* L.) and the implications for assessing the impacts of potential climate change', *European Journal of Agronomy*, vol. 2, no. 4, pp. 305-11.

Wurr, DCE & Fellows, JR 1984, 'The growth of three crisp lettuce varieties from different sowing dates', *The Journal of Agricultural Science*, vol. 102, no. 3, pp. 733-45.

Zhang, L, Hu, Z, Fan, J, Zhou, D & Tang, F 2014, 'A meta-analysis of the canopy light extinction coefficient in terrestrial ecosystems', *Frontiers of Earth Science*, vol. 8, no. 4, pp. 599-609.

Zhou, X, Zheng, HB, Xu, XQ, He, JY, Ge, XK, Yao, X, Cheng, T, Zhu, Y, Cao, WX & Tian, YC 2017, 'Predicting grain yield in rice using multi-temporal vegetation indices from UAV-based multispectral and digital imagery', *ISPRS Journal of Photogrammetry and Remote Sensing*, vol. 130, pp. 246-55.

8. APPENDIX